

Complement pathway activation mediates pancreatic cancer-induced muscle wasting and pathological remodeling

Authors: Andrew C. D'Lugos<sup>1,2</sup>, Jeremy B. Ducharme<sup>1,2,3</sup>, Chandler S. Callaway<sup>1,2</sup>, Jose G. Trevino<sup>3,4</sup>, Carl Atkinson<sup>5</sup>, Sarah M. Judge<sup>1,2,3\*</sup> & Andrew R. Judge<sup>1,2,3\*</sup>

Institutions: <sup>1</sup> Department of Physical Therapy, University of Florida, Gainesville, FL, USA.

<sup>2</sup> Myology Institute, University of Florida, Gainesville, FL, USA.

<sup>3</sup> University of Florida Health Cancer Center, Gainesville, FL, USA.

<sup>4</sup> Department of Surgery, Virginia Commonwealth University School of Medicine, Richmond, VA.

<sup>5</sup> Division of Pulmonary Medicine, University of Florida, Gainesville, FL, USA.

\*Senior and co-corresponding authors

**\*Correspondence to:**

Andrew R. Judge, Ph.D.

or

Sarah M. Judge, Ph.D.

Department of Physical Therapy

Department of Physical Therapy

University of Florida

University of Florida

Gainesville, FL 32610

Gainesville, FL 32610

P: +1 (352) 273-9220

+1 (352) 273-9146

E: arjudge@phhp.ufl.edu

E: smsenf@phhp.ufl.edu

Conflict of interest:

The authors have declared that no conflicts of interest exist.

## ABSTRACT

Cancer cachexia is a multifactorial condition characterized by skeletal muscle wasting that impairs quality of life and longevity for many cancer patients. A greater understanding of the molecular etiology of this condition is needed for effective therapies to be developed. We performed a quantitative proteomic analysis of skeletal muscle from cachectic pancreatic ductal adenocarcinoma (PDAC) patients and non-cancer controls, followed by immunohistochemical analyses of muscle cross-sections. These data provide evidence of a local inflammatory response in muscles of cachectic PDAC patients, including an accumulation of plasma proteins and recruitment of immune cells into muscle that may promote the pathological remodeling of muscle. Our data further support the complement system as a potential mediator of these processes, which we tested by injecting murine pancreatic cancer cells into wild type (WT) mice, or mice with genetic deletion of the central complement component 3 (C3<sup>-/-</sup> mice). Compared to WT mice, C3<sup>-/-</sup> mice showed attenuated tumor-induced muscle wasting and dysfunction and reduced immune cell recruitment and fibrotic remodeling of muscle. These studies demonstrate that complement activation is contributory to the skeletal muscle pathology and dysfunction in PDAC, suggesting that the complement system may possess therapeutic potential in preserving skeletal muscle mass and function.

## INTRODUCTION

Many advanced stage cancer patients suffer from the involuntary loss of body weight due to the loss of skeletal muscle mass, and often an accompanying loss of fat mass – a condition known as cachexia (1). The loss of skeletal muscle mass associates with impairments in physical function, compromising activities of daily living, independence, and quality of life; limits, or even precludes, treatment options; and is strongly predictive of early mortality (2). There is therefore a dire need for interventions to prevent or reverse cachexia in cancer patients. However, to date, the only therapy approved is in Japan, where anamorelin is approved as an appetite enhancer to counter anorexia in cachectic patients (3). One possible explanation for the current lack of therapeutics is the limited understanding of the underlying biological processes associated with muscle wasting and dysfunction in muscle from cachectic cancer patients. Without such knowledge, the successful translation of potential therapeutics may be more difficult. The more that can be learned about muscle biology and pathology from cachectic cancer patients, the better positioned therapeutics will be to target processes with established translational relevance.

In the current study, we therefore conducted unbiased total proteome profiling using multiplexed sample labeling Tandem Mass Tags (TMT) and liquid chromatography tandem mass spectrometry (LC-MS/MS) to identify proteins differentially expressed in the skeletal muscle of cachectic pancreatic cancer patients compared to non-cancer controls. We selected to study patients with pancreatic cancer due to the high prevalence of cachexia in such patients, being present in >60% of newly diagnosed patients and increasing to >80% as the disease progresses (4). We subsequently used immunohistochemical (IHC) analyses to substantiate a subset of findings from the proteome dataset using tissue sections taken from the same, and additional, cancer patients. These data identified an enrichment of complement proteins and activation of immune system processes in muscles from cachectic PDAC patients. Although the complement

system is an essential component of the host response to infection and cellular injury, playing key roles in pathogen identification, opsonization, and activation of both innate and adaptive immune cells (5), inappropriate or excessive complement activation can damage host tissues and promote inflammation (6, 7). In this regard, excessive complement activation has been implicated in the pathogenesis of various muscle diseases including dysferlinopathy, polymyositis, dermatomyositis, and inclusion body myositis (8–10). Thus, we subsequently tested the role of complement activation in cancer-induced muscle pathologies by injecting KPC pancreatic cancer cells into the pancreas of wild type mice or mice null for the central component of complement 3 (C3). Our data support the complement system as a key mediator of PDAC-induced cachexia that facilitates pathological remodeling and dysfunction of respiratory muscles, including immune cell infiltration, myofiber atrophy and fibrotic tissue remodeling.

## **RESULTS**

### **Patients**

Demographics and clinicopathological details for patients included in the proteomic analysis are presented in Table 1. All patients included in the current study were female and all PDAC patients were naïve to neoadjuvant therapy at the time of surgery. In accordance with recently published guidelines for the management of cancer cachexia (11), all PDAC patients were defined as cachectic, demonstrating involuntary body mass loss of > 5% and skeletal muscle depletion determined through CT-based measurements of skeletal muscle index, as previously described (12). In addition, the severity of cancer cachexia (grades 0-4) was determined using recently established, mortality-based criteria (13). In cases where there was insufficient sample remaining from a patient for follow on histological analyses after the proteomics, additional samples from non-cancer control (n=3) and PDAC (n=2) patients, which were not included in the initial proteomic analysis, were added. All additional patients were female and met the same

clinical (naïve to neoadjuvant therapy) and cachexia criteria as patients selected for proteomic analysis. Demographic and clinicopathological details for the expanded patient population are presented in Supplementary Table S1.

### **Pancreatic Cancer Cachexia Alters Skeletal Muscle Proteome**

The initial goal of this study aimed to characterize the skeletal muscle proteome in cachectic PDAC patients to better understand the mechanisms associated with cachexia in this population. To achieve this goal, we collected skeletal muscle biopsies of the *rectus abdominis* (n=14, Table 1). Soluble peptides from cachectic PDAC patients (n=8) and weight stable non-cancer controls (CTRL, n=6), which were separated into two pooled CTRL groups (n=3 pooled samples/group), were labeled with one of ten distinct isobaric TMT labels and annotated proteins were compared between PDAC and CTRL (Fig.1A). Following LC-MS/MS analysis, 61,463 peptides were detected among all samples, of which 44,560 peptides were uniquely identified. In total, 3,809 proteins were identified (1% FDR), of which 2,919 proteins annotated to at least 2 distinctly detected peptides. Using criteria outlined in the Methods section, 383 proteins were identified to be differentially expressed in the skeletal muscle of PDAC versus CTRL (Fig.1B, Supplemental File S2), of which 152 (39.7%) were upregulated and 231 (60.3%) were downregulated in the skeletal muscle of PDAC versus CTRL (Fig.1C).

To identify altered biological processes and pathways within the skeletal muscle of cachectic PDAC patients, differentially expressed proteins (DEPs) were analyzed using several bioinformatic platforms. Up- and downregulated proteins were analyzed separately to determine altered cellular components (Fig.1D-E) and biological processes (Fig.1F-G). The top cellular components terms enriched by proteins upregulated in muscle from PDAC patients included the membrane attack complex of the complement system, protein-transport vesicles, blood microparticles, and various components of the endoplasmic reticulum (Fig.1D). Cellular component terms enriched by proteins downregulated in muscle from PDAC patients included

various aspects of the sarcomere, including M band, I band, Z disc, muscle myosin complex, myosin filament, and troponin complex, costamere, and mitochondrial respiratory chain complex I (Fig.1E). Further *clustering* of cellular components, which condenses proteins into organized classes of proteins, to identify cellular compartments of differentially expressed proteins revealed that of the 152 DEPs that were increased, 84 annotated to *extracellular region*, 39 to *endoplasmic reticulum*, 33 to *cell junction*, 30 to *secretory vesicle*, and 18 to *blood microparticle*. When clustering the 231 DEPs that are downregulated, 87 proteins annotated to the *mitochondrion*, 40 to the *myofibril*, 14 to *sarcoplasm*, 12 to the *sarcolemma*, and 10 to *myosin complex* (Supplementary File S2).

Biological processes enriched by proteins upregulated in muscle from PDAC patients included multiple pathways of the complement system (terminal pathway of complement, alternative pathway of complement activation, regulation of complement activation), oxygen transport, protein folding in endoplasmic reticulum, and antigen presentation and processing of peptide via MHC class I (Fig. 1F). Proteins downregulated in muscle from PDAC patients showed enrichment of biological processes related to transition between fast and slow fiber, multiple aspects of muscle contraction (muscle filament sliding, regulation of striated muscle contraction, striated muscle contraction), mitochondrial processes (mitochondrial respiratory chain complex I assembly, tricarboxylic acid cycle, and electron transport chain), and metabolic processes (aspartate metabolism, malate metabolism, oxaloacetate metabolism, succinate metabolism) (Fig. 1G). Up- and downregulated proteins were analyzed together via IPA to predict activated (Fig. 1H) and inhibited (Fig. 1I) diseases and functions in PDAC skeletal muscle. Activated functions in PDAC skeletal muscle included several aspects of muscle cell death (necrosis of muscle, cell death of muscle cells, apoptosis of muscle cells, cell death of heart), movement/migration of various cell types (muscle cells, smooth muscle cells, leukocytes), synthesis and metabolism of reactive oxygen species, and fibrosis. Functions predicted as

inhibited in the skeletal muscle of PDAC predominantly included aspects of muscle contraction, as well as metabolism of amino acids, concentration of ATP, glycolysis, and cell survival.

### **Cachectic PDAC Patients Exhibit Muscle Fiber Atrophy and Collagen Remodeling**

We subsequently performed follow-up analyses using cross-sections of *rectus abdominis* from CTRL and PDAC patients to assess muscle morphology and specific biological pathways identified through proteomic analyses as dysregulated in PDAC muscle. Despite our findings of dysregulated proteins involved in “transition between fast and slow fiber” in PDAC muscle, fiber-type analyses revealed no differences in the relative abundances of myosin heavy chain (MyHC) I, IIa, and I/IIa hybrid fibers between PDAC and CTRLS (Fig.2A, B). However, upon quantification of overall muscle fiber cross-sectional area (CSA), skeletal muscle from PDAC patients exhibited a significant leftward shift towards a greater proportion of smaller muscle fibers (Fig.2C). Similarly, the CSA of each fiber type was reduced in PDAC patients versus CTRL (Fig.2D), where MyHC I, IIa, and I/IIa hybrid fibers were ~35%, ~34%, and ~33% smaller, respectively. In addition to muscle fiber atrophy, staining of muscle cross-sections with ULEX *Europeaus* Agglutinin-1 (UEA1) to identify endothelial cells (14) revealed a ~42% reduction in capillary density (total capillaries / total fibers) in PDAC versus CTRL (Fig.2E,F). This is in close agreement with recent findings from Kim et al, who also used UEA1 and found a decrease in muscle vascular density in cachectic cancer patients (15). To determine whether capillary regression occurred in a fiber-type specific manner, capillary contacts were quantified for individual MyHC I and MyHC IIa fibers. Similar to total capillary density, capillary contacts were reduced for MyHC I (~19%) and MyHC IIa (~27%) fibers in PDAC versus CTRL (Fig.2G).

In support of our previous finding of increased skeletal muscle area occupied by collagen in the *rectus abdominis* of cachectic PDAC patients (16), the unbiased proteomic analysis in the current study identified several collagen proteins to be differentially expressed in the skeletal muscle of cachectic PDAC versus CTRL (Supplemental File S2). PDAC muscle showed

reductions in the fibrillar type I collagens COL1A1 (-2.1 fold, adj  $P = 0.005$ ) and COL1A2 (-1.9 fold, adj  $P = 2.6 \times 10^{-5}$ ), in combination with reduced COL12A1 (-2.2 fold, adj  $P = 1.2 \times 10^{-6}$ ), which interacts with type I collagen and is important for muscle integrity (17). In contrast, collagen type IV, the most abundantly expressed collagen of the basement membrane in skeletal muscle tissue (18), was increased in PDAC muscle, including COL4A1 (1.4 fold, adj  $P = 6.1 \times 10^{-5}$ ) and COL4A2 (1.4 fold, adj  $P = 1.5 \times 10^{-5}$ ). To further investigate these findings and the degree of collagen remodeling, muscle cross-sections were stained for Collagen type I, Collagen type IV, and Collagen Hybridizing Peptide (CHP), a key peptide which binds only to remodeling/unfolded collagen (19) or damaged collagen fibrils (20) (Fig.2H). While the muscle area occupied by Collagen type I was not different between PDAC and CTRL, the area occupied by Collagen type IV was ~30% greater in PDAC compared to CTRL (Fig.2J). Moreover, binding of CHP was ~48% greater in PDAC compared to CTRL (Fig.2.K), suggesting increased remodeling and/or damage to existing collagen. To determine whether collagen remodeling/damage differed between collagen types, colocalization analyses were performed between CHP and collagen type I or collagen type IV. Colocalization between CHP and collagen type I was ~29% greater in PDAC versus CTRL (Fig.2L) whereas colocalization between CHP and collagen type IV was not different between groups (Fig.2M). These combined findings suggest substantial extracellular matrix (ECM) remodeling in the skeletal muscle of cachectic PDAC patients, characterized by increased remodeling/damage of collagen type I, and increased abundance of collagen type IV.

### **Complement activation in Skeletal Muscle of Cachectic PDAC Patients**

Various biological processes could lead to skeletal muscle ECM remodeling in PDAC patients, including inflammation. In this regard, the skeletal muscle proteome revealed several blood components to be elevated in muscles of cachectic PDAC patients, including albumin and other plasma proteins which are known to exit the vasculature through leaky capillaries during states of tissue and/or systemic inflammation. Of the plasma proteins increased in PDAC skeletal muscle,

proteins of the complement system, which is involved in both innate and adaptive immune responses, were highly enriched. We therefore further evaluated local indices of complement activation in PDAC muscle. To do this we first immunohistochemically analyzed skeletal muscle cross-sections for complement component 3 (C3)—the central component of complement system on which the three canonical pathways of complement activation converge. Compared to CTRL, skeletal muscle of PDAC patients showed a ~65% increase in C3 present in the muscle interstitium versus CTRL (Fig.3A,B). Moreover, C3 deposition was associated with a greater severity of cachexia, as demonstrated by a positive correlation with body weight loss (Fig.3C). Of the seven complement system proteins identified in the proteomics to be differentially expressed between CTRL and PDAC (Supplemental File S2), four are members of the terminal complement pathway, which upon activation forms the protein complex C5b-9, also known as the membrane attack complex (MAC). We therefore assessed MAC deposition in skeletal muscle cross-sections through the immunohistochemical labeling of C5b-9 (Fig.3D). Relative to CTRL, C5b-9 deposition was ~27% greater in the skeletal muscle of PDAC patients (Fig.3E). Notably, the staining pattern of C5b-9 in PDAC muscle revealed strong circumferential staining of endomysial capillaries, comparable to that observed in patients with dermatomyositis (21). In dermatomyositis, microvascular complement deposition is a suspected mechanism contributing to skeletal muscle capillary damage, inflammation, and loss of capillary density (10, 21), suggesting a similar mechanism could be at play in muscles of cachectic PDAC patients.

In addition to complement activation, we observed additional immune-related processes elevated in PDAC muscle, including “antigen presentation and processing via MHC class I”. The Major Histocompatibility Complex Class I (MHC-I) antigen presentation pathway is upregulated during innate immune responses and plays an important role in presenting intracellular antigens (peptide fragments) to CD8+ cytotoxic T cells. When the antigen displayed by MHC I on the surface of a cell is recognized as foreign (i.e. derived from pathogens, cancer cells or abnormal

cells) by CD8<sup>+</sup> T cells with specificity for that antigen, this triggers CD8<sup>+</sup> T cell responses that induce cell death. While MHC-I is typically expressed at very low levels by mature muscle cells, its upregulation in skeletal muscle is a common feature of various myopathies in which patients experience inflammation and skeletal muscle weakness (22–24). Moreover, studies have further shown that conditional upregulation of MHC-I in skeletal muscle is sufficient to drive inflammatory myositis in mice (25). We identified several components of MHC-I to be upregulated in the skeletal muscle of PDAC versus CTRL (Supplemental File.S2), including HLA class I histocompatibility antigen, A-2 alpha chain (HLA-A; 1.8 fold, adj *P* = 0.03), calreticulin (CALR; 1.5 fold, adj *P* = 0.001), calnexin (CALX; 1.4 fold, adj *P* = 0.0001), and beta-2-microglobulin (B2M; 1.8 fold, adj *P* = 0.06). In support of these findings, immunohistochemical assessment of MHC-I in muscle cross-sections revealed a 2.25-fold increased abundance in skeletal muscle of PDAC patients (Fig.3F,G). While most of the MHC-I immunoreactivity localized to cells in the interstitium, some PDAC patients also exhibited sarcolemmal staining associated with myofibers. Since a primary function of MHC-I is to present endogenous antigens on the cell surface to CD8<sup>+</sup> cytotoxic T cells (26), we hypothesized that skeletal muscle of PDAC patients may also show increased infiltration of such cells. In support of this, immunohistochemical labeling of CD3, as a T cell marker, and CD8, as a marker of cytotoxic T cells, revealed a significant 5-fold increase in cytotoxic T cells (CD3<sup>+</sup>, CD8<sup>+</sup>) in PDAC muscle cross-sections compared to CTRL (Fig.3H,I).

### **The mouse diaphragm recapitulates complement activation and fibrotic remodeling in a murine model of PDAC**

Combined, our proteomic studies and follow-up IHC studies implicate skeletal muscle microvascular depletion, and local tissue inflammation as key events that may contribute to pathological remodeling and wasting of skeletal muscles in PDAC patients exhibiting cachexia. Although the initiating triggers of these events are not entirely clear, our data suggest that the

complement system may be involved. In this regard, although transient activation of the complement system has been established to facilitate skeletal muscle regeneration following acute injury through the recruitment of monocytes/macrophages that support the regenerative process (27, 28), inappropriate or uncontrolled activation of complement can amplify inflammation and contribute to tissue injury and pathological remodeling (8, 29, 30). To build on these findings and test whether the complement system plays a causative role in mediating cancer-induced skeletal muscle pathologies we utilized the KPC pre-clinical mouse model of PDAC. In this model, KPC cells isolated from the tumor of a KPC mouse are injected into the mouse pancreas, which induces key features of PDAC-associated cachexia including myofiber atrophy and weakness (31), and pathological remodeling in the diaphragm consistent with that of PDAC patients including infiltration of leukocytes, expansion of platelet derived growth factor receptor alpha (PDGFR- $\alpha$ ) positive mesenchymal progenitors, and collagen deposition (32). Like PDAC patients, we found herein that the diaphragm muscles of KPC mice show increased C3 deposition (Fig.4A,B) that positively correlates with body weight loss (Fig.4C), and increased formation of MAC/C5b-9 complexes, including around endomysial capillaries (Fig.4D,E). Unsurprisingly, C3 deposition and MAC/C5b-9 formation were tightly correlated (Fig. 4F). In contrast, the tibialis anterior (TA) muscle did not show any increase in C3 or C5b-9 staining (Fig.4.G-J), supporting our previous findings that skeletal muscles more proximal to PDAC tumors, such as the diaphragm and the rectus abdominis muscle, show more pronounced activation of inflammatory processes and pathological remodeling compared to peripheral locomotor muscles (31–33). Through extraction of complement genes from our recently published RNA-seq dataset (32), we further show that diaphragm muscles of KPC mice exhibit upregulated transcript levels for multiple complement components and a repression in transcripts for complement inhibitors at all time points on the cachexia continuum (Fig.4K). Collectively, these data support an increase in complement pathway activation in muscles proximal to PDAC tumors in mice and people exhibiting cachexia, and suggest the involvement of *local* complement production in muscle

tissue, which could be complimentary to any systemic complement that may exit the vasculature and enter the muscle tissue . To assess systemic production of complement we also measured C3 mRNA levels in the liver, which is the major site of plasma protein production, including complement (34), and found an increase in C3 mRNA (Fig. 4L).

### **Deletion of C3 Attenuates Ascites, and Wasting of muscle and fat In a Murine Model of PDAC-Associated Cachexia**

To test the role of the complement system in PDAC-associated wasting and pathological remodeling of skeletal muscle, we injected KPC cells into the pancreas of either wild type (WT) mice or mice with genetic deletion of the central regulator of complement, C3 (C3<sup>-/-</sup> mice). At study endpoint, body mass was significantly reduced in both WT and C3<sup>-/-</sup> KPC mice relative to sham controls (Fig.5A,B). Deletion of C3 from the murine host did not impact pancreatic tumor growth (Fig.5C) or substantially impact the tumor transcriptome, as determined via RNA-sequencing of KPC tumors from WT and C3<sup>-/-</sup> mice. Indeed, only 16 genes were differentially expressed between genotypes when using adj. *P* < 0.05, which increased to only 26 genes when loosening the criteria to adj. *P* < 0.10 (Supplemental File S3). Moreover, upon extraction of previously identified marker genes that measure 14 immune cell populations (35), we found no significant differences in any of these marker genes between tumors from WT and C3<sup>-/-</sup> mice (Supplemental File S3). These data therefore support a similar overall transcriptional signature, including that reflective of the immune landscape, in KPC tumors from WT and C3<sup>-/-</sup> mice. It is important to note, however, that KPC cells injected into mice retain the C3 gene, and are thus capable of producing C3 locally within the tumor. C3 deletion from the murine host did, however, attenuate the development of peritoneal ascites (Fig.5D), a prognostic factor negatively associated with survival in PDAC patients (36). While epididymal fat mass was reduced in WT and C3<sup>-/-</sup> KPC mice (Fig.5E), the deletion of C3 imparted a 38% reduction in fat wasting compared to WT mice (Fig.5F). In

agreement with our previous findings (12), KPC tumors also induced wasting of phenotypically distinct limb musculature (Fig.6A-D), in that of the TA (Fig.6A,B) and *soleus* (SOL, Fig.6C,D). In WT mice, muscle mass was reduced by ~28% in the TA, and by ~20% in the SOL in response to KPC tumors. In contrast, in C3<sup>-/-</sup> mice KPC tumors reduced muscle mass by ~12% in the TA and ~10% in the SOL, resulting in ~50% sparing of tumor-induced muscle loss. Since muscles of cancer-free C3<sup>-/-</sup> mice were significantly smaller than WT cancer-free mice, we cannot rule out that lower starting muscle mass leads to a differential response to cachexia. However, further analysis of TA muscle fiber cross-sectional area (CSA) revealed no significant differences between cancer-free WT and C3<sup>-/-</sup> mice. In contrast, KPC tumors elicited a ~27% reduction in TA fiber CSA (Fig.6E,F) and a leftward shift in the fiber size distribution curve in WT mice (Fig.6G), which did not similarly occur in C3<sup>-/-</sup> mice (Fig.6F,G). Since transcriptional upregulation of components of the ubiquitin-proteasome and autophagy-lysosomal pathways involved in muscle protein degradation are well established to contribute to muscle wasting, including that induced by cancer (37), we measured transcript levels of several key markers of these pathways. A significant increase in the expression level of several markers of the ubiquitin-proteasome system (*Fbxo31*, *Fbxo32/Atrogin-1*, *Trim63/MuRF1*, *Psmc8*, and *Ubc*) and the autophagy-lysosomal system (*Ctsl*, *Gabrapl1*, and *Sqstm1*) was observed in the muscles of WT, but not C3<sup>-/-</sup>, KPC mice (Fig. 6H,I). Together, these data implicate the complement system as a key mediator of PDAC-induced muscle wasting. However, since we did not find evidence of complement pathway activation in the TA (a locomotor muscle) of KPC mice, these findings suggest an indirect role of complement in mediating PDAC-induced muscle wasting, at least in a peripheral locomotor muscle.

### **Deletion of C3 Ameliorates Pathological Remodeling of the Diaphragm in KPC mice**

We subsequently determined the extent to which the complement system mediates KPC-induced wasting, inflammation and pathological remodeling of the diaphragm, which unlike locomotor muscles shows evidence of complement pathway activation similar to *rectus abdominis* muscles from cachectic PDAC patients. Cross-sections of costal diaphragm were subjected to immunohistochemical staining of myosin heavy chain (MyHC) I, MyHC IIa, and wheat germ agglutinin to assess fiber type-specific muscle fiber size (Fig.7A-I). In WT mice, KPC tumors induced atrophy of MyHC I fibers (~29%, Fig.7B), MyHC I/IIa hybrid fibers (~26%, Fig.7C), MyHC IIa fibers (~26%, Fig.7D), and MyHC IIx/IIb fibers (~33%, Fig.7E). Similar to locomotor muscles, diaphragm muscles from C3<sup>-/-</sup> mice were protected from KPC-induced muscle fiber atrophy (Fig.7B-E).

We recently identified an increase in infiltrating leukocytes in the diaphragm of KPC mice that occurs prior to the onset of cachexia and continues throughout cachexia progression (32). Given that a key role of complement activation is to facilitate immune cell chemotaxis to local sites of complement activation (38), including in skeletal muscle (28, 39), we next stained diaphragm cross-sections with CD45, a pan-leukocyte marker (Fig.8A), to determine whether the complement system mediates immune cell trafficking into the diaphragm of KPC mice. The diaphragm of WT KPC mice exhibited an ~10-fold increase in infiltrating leukocytes, which was attenuated in mice lacking C3 (Fig.8B). Since non-resolute inflammation can contribute to the expansion of fibroadipogenic progenitor (FAP) cells (40) and fibrotic remodeling of muscle, and we recently showed that leukocyte infiltration and inflammatory processes within the diaphragm of KPC mice precedes the expansion of FAPs and fibrosis (32), we further assessed the impact of C3 deletion on the expansion of PDGFR $\alpha$ <sup>+</sup> FAPs, ECM expansion and collagen deposition within the diaphragm. While KPC tumors caused a robust increase in the abundance of PDGFR $\alpha$ <sup>+</sup> FAP cells in the diaphragm of both genotypes, C3<sup>-/-</sup> mice showed significantly attenuated (~43%) FAP cell abundance (Fig.8C,D). Deletion of C3 also mitigated the expansion in muscle area

occupied by collagen (Fig. 8E,F), and total ECM as measured via staining with wheat germ agglutinin (WGA; Fig. 8G). Correlative analysis between FAP cells and muscle area occupied by collagen across genotypes revealed a significant, positive relationship ( $P = 0.0002$ ,  $R = 0.61$ , Fig.8H) supporting the notion that FAP expansion is closely linked to the fibrofatty remodeling of respiratory muscles in pancreatic tumor bearing hosts. Collectively, these findings suggest that in addition to complement regulating systemic wasting of muscles in response to PDAC, local complement activation in skeletal muscles proximal to the tumor, such as the diaphragm, may be a key mediator of leukocyte infiltration, FAP expansion and replacement of muscle with fibrofatty tissue.

### **Deletion of C3 Preserves *In-Vivo* and *Ex-Vivo* Diaphragm Function in Response to KPC Tumors**

Since C3 deletion mitigated several indices of diaphragm pathology in KPC mice, we subsequently determined whether this translates to preservation of respiratory and contractile function (12, 31, 32). *In-vivo* diaphragm function was indirectly assessed, non-invasively, at study endpoint using M-mode ultrasonography (Fig.9A). KPC tumors reduced diaphragm excursion by ~37% in WT mice, but not in C3<sup>-/-</sup> mice (Fig.9B). Respiratory rate (Fig.9C) and estimated minute ventilation (Fig.9D) were also decreased in WT mice but spared in C3<sup>-/-</sup> mice. It is worth noting, however, that C3<sup>-/-</sup> sham mice showed ~50% reduction in both respiratory rate and minute ventilation compared to WT shams, despite no overt phenotype and, to the best of our knowledge, exhibiting no known respiratory deficits. To evaluate diaphragm contractile function more directly, we measured the *ex-vivo* contractile mechanics of costal diaphragm from WT and C3<sup>-/-</sup> KPC mice (Fig.9E-G). Relative to WT KPC mice, the maximal normalized force of the diaphragm from C3<sup>-/-</sup> KPC mice was ~51% greater (Fig.9F). In addition, diaphragm from C3<sup>-/-</sup> KPC mice generated greater tetanic forces across a range of stimulation frequencies compared to diaphragm from WT

KPC mice (Fig.9G). Together with our histological data, these findings suggest that excessive complement activation in the diaphragm may be a key mediator of local inflammation and pathological replacement of muscle with fibrofatty tissue in response to PDAC that may contribute to muscle dysfunction—with strong translational relevance to patients.

## **DISCUSSION**

The present study builds on previously published findings from our laboratory using muscle biopsies from cachectic PDAC patients, that identified a pathological progression towards the replacement of muscle with fat and fibrotic tissue that was associated with areas of immune cell infiltration and expansion of FAPs (16). Through unbiased proteomics herein we further identified multiple proteins and biological processes associated with these pathologies, providing additional insight into underlying mechanisms that may be involved.

Using Masson's Trichrome staining on skeletal muscle cross sections, we previously discovered that the total muscle area occupied by collagen was increased in cachectic PDAC patients compared to non-cachectic PDAC patients and non-cancer controls, and was associated with poor survival (16). In the current study, using unbiased proteomics and follow-up IHC analyses, we found that the expansion of muscle area occupied by collagen in cachectic PDAC may be attributed to increased abundance of Collagen IV. Collagen IV is highly abundant in skeletal muscle tissue and the primary collagen of the basement membrane, which surrounds muscle fibers and is critical for both structure and the physiological function of muscle (41). It is also the membrane under which satellite cells reside and plays a key role in the regeneration of muscle (42). Thus, any change in collagen IV levels has the potential to alter muscle structure and function, as well as satellite cell biology and muscle regeneration, all of which have been shown to be altered in the muscles of tumor bearing hosts (43, 44). In contrast to Collagen IV, proteomics analyses revealed decreased abundance of collagen type I alpha 1 and 2 chain proteins, despite

no changes in the total muscle area occupied by collagen type I via IHC. However, muscle from PDAC patients exhibited increased co-localization of collagen type I with the collagen hybridizing peptide (CHP), which has a high propensity for binding to unfolded collagen chains, and is used experimentally to detect, localize, and compare molecular damage and/or denaturation of collagen (20, 45). The finding that collagen I within muscle tissue is molecularly damaged in cachectic PDAC patients is not entirely surprising given that inflammatory processes were highly upregulated in muscles from these patients. Indeed, an abundance of literature exists supporting inflammation as a key trigger of collagen degradation within the ECM (46–48), with subsequent remodeling and expansion of the ECM occurring as an adaptive response to stabilize the damaged tissue. Consequentially, muscle tissue inflammation and damage to collagen I, which confers tensile strength and rigidity to the muscle (49), has the potential to negatively impact muscle structure and function, including via increasing the susceptibility to contraction-induced injury which we have previously demonstrated occurs in respiratory muscles of tumor bearing mice (12).

In addition to ECM remodeling, cachectic PDAC patients also displayed myofiber atrophy, which is a defining characteristic of cancer cachexia. Here, we found a significant and comparable, 33-35%, decrease in the cross-sectional area of Type I, Type IIa and Type I/IIa hybrid fibers of cachectic PDAC patients compared to controls. This is in close agreement with previously published data in the rectus abdominis muscle from upper gastrointestinal or pancreatic cancer patients, which showed a ~26% decrease in the cross-sectional area of both Type I and Type IIa myofibers (50). We similarly did not find any evidence of a fiber type specific difference in capillary contacts, with reduced capillary contacts for both Type I and IIa fibers in PDAC patients compared to non-cancer controls. As alluded to previously, since capillaries deliver oxygen, nutrients, and growth factors that are essential to muscle health, a decrease in vascular density could be a trigger that disrupts muscle homeostasis. Indeed, in aging a decrease in vascular density has

been linked to anabolic resistance and a decrease in muscle mass and strength (51, 52), each of which have been demonstrated in cancer cachexia. Moreover, adequate skeletal muscle capillarization is also vital for satellite cell function and muscle regeneration (53, 54), a process that is impaired in cancer cachexia (44). Thus, a decrease in muscle capillary density could be causative in several pathological features of cancer cachexia, which clearly warrants further study.

Our data suggest that both innate and adaptive immune-system processes, and the complement system, are activated in muscle of cachectic PDAC patients and may play a key role in driving wasting, inflammation, and pathological remodeling of skeletal muscle. Excessive activation of complement is associated with muscle wasting and pathological remodeling in a number of conditions, including ischemia-reperfusion injury (6) and autoimmune and inflammatory diseases (7), through promoting inflammation and host tissue damage. Inappropriate activation of complement has also been identified as a driver of macrophage infiltration into skeletal muscle, and muscle weakness, in amyotrophic lateral sclerosis (39, 55), and is implicated in the pathogenesis of dysferlinopathy (8), and a number of other muscle diseases including myasthenia gravis (56, 57), polymyositis, dermatomyositis and inclusion body myositis (9, 10), and X-linked vacuolated myopathy (58). Our findings herein add to this body of knowledge by demonstrating complement activation in skeletal muscle of cachectic PDAC patients. Through our pre-clinical modeling of PDAC cachexia using the orthotopic KPC model, we demonstrate that the complement system also mediates leukocyte infiltration and pathological remodeling of the diaphragm—a murine muscle which we have shown recapitulates key aspects of muscle pathology observed in cachectic PDAC patients (33). Indeed, blockade of complement activation through deletion of C3 significantly deterred leukocyte infiltration into the diaphragm and inhibited the expansion of FAPs and the muscle ECM, supporting local complement activation as a key driver of respiratory muscle inflammation and pathological remodeling. While the initiating signals

inciting complement activation in PDAC cachexia is not clear, local production/release of damage/danger-associated molecular patterns (DAMPs) from damaged or dying cells within the muscle could be involved (59). In this regard, we and others have previously demonstrated evidence of myofiber damage and sarcolemmal disruption in muscles of cachectic PDAC patients (16, 60). Our data also support an indirect role of complement activation in mediating the cachexia syndrome, as deletion of C3 also reduced whole-body wasting of muscle and fat, despite no effects on tumor size, and minimal effects on the tumor transcriptome. However, since complement activation can be initiated by three pathways, and each converge on C3, our studies do not distinguish which of these pathway(s) are involved in cancer cachexia. Rather, the findings presented herein lay the foundation to further dissect the specific pathways involved in complement activation that mediate the cachexia phenotype.

The findings herein are supported by previous work which found that muscle, fat, and plasma complement levels associate with cachexia in pancreatic cancer patients. In this regard, increasing levels of complement component C4A mRNA in both muscle and adipose tissue were found to correlate with increased cancer weight loss grade in PDAC patients (61), while C3a, a cleavage product of C3, was recently shown to be significantly higher in plasma from cachectic pancreatic cancer patients with inflammation compared to those without cachexia (62). Notably, the complement pathway is also associated with cachexia induced by other cancer types and in response to chemotherapy. Indeed in colon adenocarcinoma 26 (C26) tumor bearing mice, the complement pathway was identified as the most enriched pathway from genes upregulated in the muscle of both moderately and severely cachectic mice (63), with C3 protein levels found to also be increased in the muscle of cachectic C26 mice and in mice undergoing cachexia in response to Folfiri chemotherapy treatment (64). The complement system was also identified as an enriched pathway from genes upregulated in the muscles of cachectic mice bearing Lewis lung

tumors (65). Thus, upregulation of the complement system is a common finding in cachectic tumor bearing hosts.

Importantly, several FDA-approved complement inhibitors are currently available that are mostly used in rare diseases such as Paroxysmal Nocturnal Hemoglobinuria, Geographic Atrophy, anti-neutrophil cytoplasmic autoantibody (ANCA)-associated vasculitis, and Hereditary Angioedema (66, 67). These inhibitors block complement activity at different stages of the activation pathway and include Pegcetacoplan and Eculizumab, which systemically bind and block cleavage of complement C3 and C5, respectively; Berinert and Sutimlimab, which block early complement activation by inhibiting C1s/1r and mannose binding associated serum proteases (MASPs) and; Avacopan which inhibits the activation of C5a by antagonism of the C5a receptor. Interestingly, a randomized phase II trial at Roswell Park Comprehensive Cancer Center is currently testing the effect of pegcetacoplan when given in combination with the programmed death-1 (PD-1) inhibitor pembrolizumab, or when given in combination with pembrolizumab plus bevacizumab, an inhibitor of vascular endothelial growth factor (VEGF), in patients with ovarian, fallopian tube, or primary peritoneal cancer. The premise is based on the potential for pegcetacopla to enhance anti-tumor activity by reducing immunosuppression in the tumor microenvironment when used in combination with immunotherapies. Thus, complement therapeutics hold potential as part of a multifaceted approach to cancer treatment.

In summary, we identified local complement deposition and activation in skeletal muscle of cachectic PDAC patients as a potentially key initiator of muscle inflammation and pathological replacement of muscle with fibrofatty tissue. Importantly, analyses were performed on skeletal muscle biopsies obtained from treatment-naïve patients at the beginning of their tumor resection surgery, which supports the cancer and not the surgery or therapy, as an explanation for these findings. Our findings are supported through the use of a complimentary murine PDAC model, in which we demonstrate that respiratory muscles from PDAC mice deficient in complement

activation show marked reductions in immune cell infiltration, expansion of fibroadipogenic progenitors and ECM/collagen expansion compared to WT mice. Lastly, our data suggest a key role for complement activation in mediating whole-body cachexia, based on our finding that PDAC mice deficient in complement also showed attenuation in whole body wasting of muscle and fat.

## **METHODS**

### **Sex as a biological variable**

Our tissue bank contained more muscle tissues from female patients naïve to neoadjuvant therapy than it did male patients naïve to neoadjuvant therapy. To reduce the number of variables (such as sex and therapy) for the proteome study, we therefore chose to examine muscles collected from female patients only. Interestingly, although the lytic pathway is equally robust in female and male humans, the lytic pathway is not robust in female mice. Therefore, in our mouse studies, we selected to study male mice.

### **Patient samples**

Skeletal muscle biopsies of the *rectus abdominis* were obtained from eligible patients following a prospective collection model, as previously described (16). Briefly, portions of each skeletal muscle sample were either flash frozen in liquid nitrogen (for proteomic analyses) or embedded in optimal cutting temperature (OCT) compound and frozen in liquid nitrogen-cooled isopentane. All samples were stored at -80°C until further analyses.

The eligible population consisted of confirmed PDAC patients undergoing surgical resection with curative intent and weight-stable patients undergoing benign abdominal surgery as non-cancer controls at the University of Florida Pancreatic Surgical Center between March 2015 and September 2017. Demographics and clinicopathological details of patients are included in Table 1 and Supplementary Table S1. All patients were female, and all PDAC patients were naïve to

neoadjuvant therapy at the time of surgery and were defined as cachectic, with >5% involuntary body mass loss and skeletal muscle depletion measured via CT-based skeletal muscle index (12). Samples from 8 PDAC patients and 6 non-cancer control patients were included for proteomic analyses. In cases where there was insufficient sample remaining from a patient for follow on histological analyses after the proteomics, additional samples from non-cancer control (n=3) and PDAC (n=2) patients, which were not included in the initial proteomic analysis, were added.

### **Proteomic analysis**

The methodological workflow of proteomic analyses is displayed in Figure 1. Protein isolation and quantitative proteomics were performed by Cell Signaling Technologies (Danvers, MA), as previously described (68), and detailed methods are included in Supplemental Methodology. Samples from cachectic PDAC patients and non-cancer controls were labeled with Tandem Mass Tag (TMT) reagents (Thermo Fisher Scientific, Waltham, MA) and labelled samples were fractionated using basic reverse phase (bRP) fractionation chromatography. A total of 96 bRP fractions were collected over the entire gradient and multiplexed using a TMT10plex (Thermo Fisher Scientific). Samples were analyzed on an Orbitrap Fusion Lumos Tribrid mass spectrometer (Thermo Fisher Scientific). Peptide-spectral matching was performed using a target-decoy strategy and linear discriminant analysis (LDA) at a 2% false discovery rate (FDR), with protein identification filtered to a 1% FDR. The mass spectrometry data have been deposited in the ProteomeXchange Consortium via the PRIDE repository (PXD047838).

Differences in protein abundance between PDAC and CTRL were determined by comparing the summed signal-to-noise ratios and significance was assessed using a nonparametric independent samples t-test. The *P*-values were corrected with the Benjamini-Hochberg method and relative protein abundance was expressed as fold change (FC) relative to CTRL. Proteins were classified as differentially expressed between PDAC and CTRL if they met the following criteria: detected peptides  $\geq 2$ , adjusted *P*-value (FDR)  $\leq 0.05$ , median FC of  $>1.25$

or  $<-1.25$ , same directional FC in  $\geq 5$  PDAC patients. The latter criteria for differential expression classification was implemented in an attempt to identify biological targets altered in a broader patient population.

## **Animals**

Mice were provided *ad libitum* access to standard chow and water and housed in a temperature- and humidity-controlled facility on a 12-hour light/dark cycle. Twelve-week-old male C57Bl/6J mice (WT; stock no: 000664) and complement C3 null mice (C3<sup>-/-</sup>; stock no: 029661 (69)) were purchased from The Jackson Laboratory.

## **Cancer cachexia model**

KPC FC1245 pancreatic cancer cells (obtained from Dr. David Tuveson, Cold Spring Harbor Laboratory, Cold Spring Harbor, NY, and isolated from the tumor of a *LSL-KrasG12D/+;LSL-Trp53<sup>R172H/+</sup>;Pdx-1-Cre* mouse) were maintained in DMEM supplemented with 10% FBS, 1% penicillin, and 1% streptomycin in a humidified chamber at 37°C and 5% CO<sub>2</sub>. For injection into mice, the pancreas was surgically exposed and its tail injected with  $0.25 \times 10^6$  KPC cells diluted in 50  $\mu$ L of sterile PBS (KPC), or 50  $\mu$ L of sterile PBS alone (SHAM). Mice were monitored daily and euthanized when WT KPC bearing mice reached IACUC-mandated experimental endpoint, based on body condition score and tumor size.

## ***In-vivo* assessment of diaphragm function**

A wide-band phased-array ultrasound transducer (6S-RS, GE Healthcare) was positioned transverse on the abdomen of anesthetized mice, immediately distal to the xiphoid process, angled superiorly toward the diaphragm and thoracic cavity, ensuring no compression of the abdominal cavity. After a standardized duration of anesthesia was achieved, at least three M-mode video traces of the diaphragm were acquired (LOGIQ e Vet NEXTGEN, GE Healthcare).

Each video recorded 10 seconds of tidal breathing to measure excursion amplitude and breathing frequency, with measurements averaged per animal.

### ***Ex-vivo* muscle function assessment**

*Ex-vivo* contractile function was assessed at the Physiological Assessment Core of the University of Florida as previously described (70) from WT and C3<sup>-/-</sup> tumor-bearing mice. Briefly, at IACUC-mandated tumor-endpoint, freshly isolated costal diaphragm strips were mounted on a force transducer (dual-mode lever system – Aurora Scientific, Ontario, Canada) placed in a 22°C Ringers solution bath equilibrated with 95% O<sub>2</sub> and 5% CO<sub>2</sub>. After determining optimal muscle length, maximum isometric twitch and tetanic forces were measured using a single supramaximal stimulation and a 500-ms train at 150 Hz, respectively, with a 5-min rest period between each set. Subsequently, diaphragm strips were stimulated at frequencies ranging from 5-150 Hz to establish a force-frequency relationship.

### **Immunohistochemical analyses**

Transverse 7- $\mu$ m thick cross-sections were cut from skeletal muscle samples previously embedded in OCT medium and frozen in liquid nitrogen-cooled isopentane. Sections were cut at -20°C and mounted onto uncoated glass slides. Slides were air dried and stored at -80°C until further analysis.

Skeletal muscle cross-sections from PDAC and CTRL patients were processed for gross morphological features including fiber type-specific myofiber size and typology, as well as fiber type-specific capillary content. Subsequent immunofluorescent assays were guided by bioinformatics of the unbiased proteomic analysis. Briefly, the abundance of collagen type I, collagen type IV, and collagen hybridizing peptide (CHP) were assessed as previously described (71). Expression of major histocompatibility complex class I (MHC-I) was quantified and subsequently, the abundance of CD3<sup>+</sup> T cells and CD3<sup>+</sup>/CD8<sup>+</sup> cytotoxic T cells were assessed.

Activation of the complement system was measured by quantifying the central regulator of complement, component C3, as well as formation of the terminal arm of complement, the membrane attack complex (MAC; C5b-9).

Cross-sections of mouse limb (TA) and respiratory (DIA) muscle were subjected to hematoxylin and eosin staining to assess gross morphology (33) and picosirius red staining to assess collagen content. Myofiber size was quantified in both muscles, whereas fiber typology was quantified in the DIA given its relatively heterogenous fiber type profile compared to the TA. Infiltrating leukocytes were quantified through CD45 staining in both muscles and the expansion of the fibroadipogenic progenitor cell population was assessed by staining for platelet-derived growth factor receptor alpha, as previously described (32). Detailed information on the methodologies and reagents used can be found in Supplemental File S1 and Supplementary Table S2.

### **Image acquisition and analysis**

Immunofluorescent analyses of PDAC and CTRL skeletal muscle samples, including fiber type-specific myofiber size and capillarization, expression of MHC-I, and deposition of complement C3 and C5b-9 (MAC) were acquired at 100x total magnification with an upright fluorescent microscope equipped with a digital camera (DM5000B, Leica, Wetzlar, Germany). Whole cross-sectional images of PDAC and CTRL samples stained for collagen I, collagen IV, CHP, and CD3<sup>+</sup> and CD8<sup>+</sup> T cells were acquired using a TCS SP8 confocal microscope (Leica). For colocalization analyses, images of collagen I, collagen IV, and CHP were acquired at 200x total magnification (0.75 numerical aperture objective). Pixel intensity thresholds were set using single-labeled control samples as described previously (72) and all imaging parameters were kept constant for all samples. H&E and picosirius red staining was imaged with brightfield microscopy (DM5000B, Leica) at 200x total magnification. All subsequent immunofluorescent staining of mouse TA and DIA was acquired as whole cross-sectional images on a confocal microscope

(Leica) at 200x total magnification. Colocalization analyses were performed on deconvolved images using LAS X software (Leica). All other image analysis was performed in FIJI.

### **RNA isolation, cDNA synthesis, RT-qPCR, and RNA-sequencing**

For RNA isolation, TA muscles or KPC tumors were homogenized in Trizol, followed by chloroform extraction, isopropanol precipitation, and DNase treatment (AM1906, Invitrogen). Integrity of RNA was assessed with a Bioanalyzer 2100 (Agilent Technologies, Santa Clara, CA). From TA muscles, 1 µg of RNA was reverse transcribed using the iScript Advance cDNA Synthesis kit (Bio-Rad, Hercules, CA). Cycle thresholds were measured via fluorometric PCR (QuantStudio 3, Applied Biosystems, Waltham, MA) on the generated cDNA using TaqMan probes listed in Supplemental Table S2 and quantified using the  $2^{-\Delta\Delta Ct}$  method with *18S* as the reference gene. RNA from KPC tumors was sent to Novogene (Sacramento, CA) for RNA-seq analysis. A total of 1 µg of RNA per sample was used to generate sequencing libraries which were sequenced on Novogene's Illumina NovaSeq 6000 (2×150bp) to achieve at least 40M reads per sample. Paired-end reads were aligned to the *Mus musculus* genome (mm39) using STAR (v2.5) and annotated with HTseq-counts (v0.6.1). Differential expression was analyzed with DESeq2 (v1.20.0), and adjusted *P*-values were calculated using the Benjamini-Hochberg method. Genes with adj. *P*-value < 0.05 were considered differentially expressed. RNA-seq data from KPC tumors is available at GSE274179.

### **Extraction of complement genes from diaphragm RNA-seq data**

Genes involved in complement signaling were extracted from our recently published bulk RNA-seq dataset from diaphragm muscles of Sham mice and from KPC tumor-bearing mice collected at various time points throughout the cachexia trajectory ((32) and GSE271521).

### Bioinformatic analyses

Enrichment analyses were performed using DAVID (73), String (74), and Ingenuity Pathway Analysis (75) platforms.

### **Statistics**

Statistical analyses were performed using GraphPad Prism (v8, San Diego, CA). Data were tested for normality with the Shapiro-Wilk test. Comparisons between two groups were made with a Student's two-tailed t-test or Mann-Whitney U test. For comparisons involving more than two groups, a two-way ANOVA was performed with Sidak post hoc analysis. Correlations were assessed using linear regression. A *P*-value < 0.05 was considered significant.

### **Study Approval**

The inclusion of human subjects was approved by the University of Florida Institutional Review Board and written informed consent was obtained from all participants. All animal procedures were performed in accordance with NIH guidelines and with the approval of the University of Florida IACUC.

### **Data availability**

All data generated in this study are available in public databases (RNA-seq: GSE274179; mass spectrometry: PXD047838) or in Supplemental File S4 as supporting data values.

## **AUTHOR CONTRIBUTIONS**

ACD, SMJ, and ARJ conceived the study; ACD, JBD, CSC, CA, SMJ, and ARJ participated in data acquisition, analysis and interpretation; JGT collected the human samples; ACD, JBD, CA, JGT, SMJ, and ARJ drafted the manuscript and have primary responsibility for final content. All authors read and approved the submitted version and have agreed to be personally accountable for the author's own contributions and to ensure that questions related to the accuracy or integrity of any part of the work are appropriately investigated and resolved.

## **ACKNOWLEDGEMENTS**

This work was supported by the National Institute of Arthritis, Musculoskeletal and Skin Diseases (R01AR060209 to ARJ, R01AR081648 to ARJ and CA (MPI)), the National Cancer Institute (NCI) (R01CA270025 to SMJ) and the Circle of Hope for Cancer Research Inc. (Young Investigator Research Grant to ACD). ACD was supported by a National Heart, Lung and Blood Institutional training grant (T32HL134621). JBD is supported by an NCI training grant (T32CA257923) and the UF Health Cancer Center, which is supported in part by state appropriations provided in Fla. Stat. § 381.915 and the NCI (P30CA247796). The authors would like to thank the Physiological Assessment Core of the University of Florida, which was established under the Senator Paul D. Wellstone Muscular Dystrophy Cooperative Research Center (P50AR052646 to H. Lee Sweeney), for performing *ex-vivo* muscle contractility experiments, and all the patients for their participation in this study.

## REFERENCES

1. Baracos VE, et al. Cancer-associated cachexia. *Nat Rev Dis Primers*. 2018;4:17105.
2. Kazemi-Bajestani SMR, Mazurak VC, Baracos V. Computed tomography-defined muscle and fat wasting are associated with cancer clinical outcomes. *Semin Cell Dev Biol*. 2016;54:2–10.
3. Wakabayashi H, Arai H, Inui A. The regulatory approval of anamorelin for treatment of cachexia in patients with non-small cell lung cancer, gastric cancer, pancreatic cancer, and colorectal cancer in Japan: facts and numbers. *J Cachexia Sarcopenia Muscle*. 2021;12(1):14–16.
4. Kahl C, et al. Long-term follow-up of the AML97 study for patients aged 60 years and above with acute myeloid leukaemia: a study of the East German Haematology and Oncology Study Group (OSHO). *J Cancer Res Clin Oncol*. 2016;142(1):305–315.
5. Dunkelberger JR, Song W-C. Complement and its role in innate and adaptive immune responses. *Cell Res*. 2010;20(1):34–50.
6. Mollnes TE, Song W-C, Lambris JD. Complement in inflammatory tissue damage and disease. *Trends Immunol*. 2002;23(2):61–64.
7. Tsokos GC, Fleming SD. Autoimmunity, Complement Activation, Tissue Injury and Reciprocal Effects. 2003;7:149–164.
8. Han R, et al. Genetic ablation of complement C3 attenuates muscle pathology in dysferlin-deficient mice. *J Clin Invest*. 2010;120(12):4366–4374.
9. Dalakas MC. Polymyositis, dermatomyositis and inclusion-body myositis. *N Engl J Med*. 1991;325(21):1487–1498.
10. Emslie-Smith AM, Engel AG. Microvascular changes in early and advanced dermatomyositis: a quantitative study. *Ann Neurol*. 1990;27(4):343–356.
11. Roeland EJ, et al. Management of Cancer Cachexia: ASCO Guideline. *J Clin Oncol*. 2020;38(21):2438–2453.
12. Judge SM, et al. MEF2c-dependent downregulation of Myocilin mediates cancer-induced muscle wasting and associates with cachexia in cancer patients. *Cancer Res*. 2020;80(9):1861–1874.
13. Martin L, et al. Diagnostic criteria for the classification of cancer-associated weight loss. *J Clin Oncol*. 2015;33(1):90–99.
14. Holthöfer H, et al. Ulex europaeus I lectin as a marker for vascular endothelium in human tissues. *Lab Invest*. 1982;47(1):60–66.
15. Kim Y-M, et al. Impaired Barrier Integrity of the Skeletal Muscle Vascular Endothelium Drives Progression of Cancer Cachexia [preprint]. 2022;2022.12.12.520118.
16. Judge SM, et al. Skeletal Muscle Fibrosis in Pancreatic Cancer Patients with Respect to Survival. *JNCI Cancer Spectr*. 2018;2(3):pky043.
17. Bader HL, et al. Zebrafish collagen XII is present in embryonic connective tissue sheaths (fascia) and basement membranes. *Matrix Biol*. 2009;28(1):32–43.
18. Gillies AR, Lieber RL. Structure and function of the skeletal muscle extracellular matrix. *Muscle Nerve*. 2011;44(3):318–331.
19. Hwang J, et al. In Situ Imaging of Tissue Remodeling with Collagen Hybridizing Peptides. *ACS Nano*. 2017;11(10):9825–9835.
20. Zitnay JL, et al. Molecular level detection and localization of mechanical damage in collagen enabled by collagen hybridizing peptides. *Nat Commun*. 2017;8:14913.
21. Lahoria R, Selcen D, Engel AG. Microvascular alterations and the role of complement in dermatomyositis. *Brain*. 2016;139(Pt 7):1891–1903.
22. Vogel H, Zamecnik J. Diagnostic immunohistology of muscle diseases. *J Neuropathol Exp Neurol*. 2005;64(3):181–193.

23. Lundberg IE. The physiology of inflammatory myopathies: an overview. *Acta Physiol Scand.* 2001;171(3):207–213.
24. Appleyard ST, et al. Increased expression of HLA ABC class I antigens by muscle fibres in Duchenne muscular dystrophy, inflammatory myopathy, and other neuromuscular disorders. *The Lancet.* 1985;325(8425):361–363.
25. Nagaraju K, et al. Conditional up-regulation of MHC class I in skeletal muscle leads to self-sustaining autoimmune myositis and myositis-specific autoantibodies. *Proc Natl Acad Sci U S A.* 2000;97(16):9209–9214.
26. York IA, Rock KL. Antigen processing and presentation by the class I major histocompatibility complex. *Annu Rev Immunol.* 1996;14:369–396.
27. Tidball JG. Interactions between muscle and the immune system during modified musculoskeletal loading. *Clin Orthop Relat Res.* 2002;(403 Suppl):S100-109.
28. Zhang C, et al. Complement C3a signaling facilitates skeletal muscle regeneration by regulating monocyte function and trafficking. *Nat Commun.* 2017;8(1):2078.
29. Ricklin D, Reis ES, Lambris JD. Complement in disease: a defence system turning offensive. *Nat Rev Nephrol.* 2016;12(7):383–401.
30. Dalakas MC, Alexopoulos H, Spaeth PJ. Complement in neurological disorders and emerging complement-targeted therapeutics. *Nat Rev Neurol.* 2020;16(11):601–617.
31. Neyroud D, et al. Blocking muscle wasting via deletion of the muscle-specific E3 ligase MuRF1 impedes pancreatic tumor growth. *Commun Biol.* 2023;6(1):519.
32. Neyroud D, et al. Local Inflammation Precedes Diaphragm Wasting and Fibrotic Remodelling in a Mouse Model of Pancreatic Cancer. *J Cachexia Sarcopenia Muscle.* 2025;16(1):e13668.
33. Nosacka RL, et al. Distinct cachexia profiles in response to human pancreatic tumours in mouse limb and respiratory muscle. *J Cachexia Sarcopenia Muscle.* 2020;11(3):820–837.
34. Qin X, Gao B. The complement system in liver diseases. *Cell Mol Immunol.* 2006;3(5):333–340.
35. Danaher P, et al. Gene expression markers of Tumor Infiltrating Leukocytes. *J Immunother Cancer.* 2017;5:18.
36. Baretti M, et al. The Significance of Ascites in Patients With Pancreatic Ductal Adenocarcinoma: A Case-Control Study. *Pancreas.* 2019;48(4):585–589.
37. Martin A, Gallot YS, Freyssenet D. Molecular mechanisms of cancer cachexia-related loss of skeletal muscle mass: data analysis from preclinical and clinical studies. *J Cachexia Sarcopenia Muscle.* 2023;14(3):1150–1167.
38. Markiewski MM, Lambris JD. The role of complement in inflammatory diseases from behind the scenes into the spotlight. *Am J Pathol.* 2007;171(3):715–727.
39. Wang HA, et al. Complement C5a-C5aR1 signalling drives skeletal muscle macrophage recruitment in the hSOD1G93A mouse model of amyotrophic lateral sclerosis. *Skelet Muscle.* 2017;7(1):10.
40. Santini MP, et al. Tissue-Resident PDGFR $\alpha$ + Progenitor Cells Contribute to Fibrosis versus Healing in a Context- and Spatiotemporally Dependent Manner. *Cell Rep.* 2020;30(2):555-570.e7.
41. Campbell KP, Stull JT. Skeletal muscle basement membrane-sarcolemma-cytoskeleton interaction minireview series. *J Biol Chem.* 2003;278(15):12599–12600.
42. Zhang W, Liu Y, Zhang H. Extracellular matrix: an important regulator of cell functions and skeletal muscle development. *Cell Biosci.* 2021;11(1):65.
43. He WA, et al. NF- $\kappa$ B-mediated Pax7 dysregulation in the muscle microenvironment promotes cancer cachexia. *J Clin Invest.* 2013;123(11):4821–4835.
44. Talbert EE, Guttridge DC. Impaired regeneration: A role for the muscle microenvironment in cancer cachexia. *Semin Cell Dev Biol.* 2016;54:82–91.

45. Li Y, et al. Targeting collagen strands by photo-triggered triple-helix hybridization. *Proc Natl Acad Sci U S A*. 2012;109(37):14767–14772.
46. Cui S-J, et al. Chronic inflammation deteriorates structure and function of collagen fibril in rat temporomandibular joint disc. *Int J Oral Sci*. 2019;11(1):2.
47. Li J, et al. Collagen degradation in a murine myocarditis model: relevance of matrix metalloproteinase in association with inflammatory induction. *Cardiovasc Res*. 2002;56(2):235–247.
48. Pfisterer K, et al. The Extracellular Matrix in Skin Inflammation and Infection. *Front Cell Dev Biol*. 2021;9:682414.
49. Kovanen V. Intramuscular extracellular matrix: complex environment of muscle cells. *Exerc Sport Sci Rev*. 2002;30(1):20–25.
50. Johns N, et al. Clinical classification of cancer cachexia: phenotypic correlates in human skeletal muscle. *PLoS One*. 2014;9(1):e83618.
51. Moro T, et al. Low skeletal muscle capillarization limits muscle adaptation to resistance exercise training in older adults. *Exp Gerontol*. 2019;127:110723.
52. Banks NF, et al. The contributory role of vascular health in age-related anabolic resistance. *J Cachexia Sarcopenia Muscle*. 2022;13(1):114–127.
53. Christov C, et al. Muscle satellite cells and endothelial cells: close neighbors and privileged partners. *Mol Biol Cell*. 2007;18(4):1397–1409.
54. Abou-Khalil R, Mounier R, Chazaud B. Regulation of myogenic stem cell behavior by vessel cells: the “ménage à trois” of satellite cells, periendothelial cells and endothelial cells. *Cell Cycle*. 2010;9(5):892–896.
55. Bahia El Idrissi N, et al. Complement activation at the motor end-plates in amyotrophic lateral sclerosis. *J Neuroinflammation*. 2016;13(1):72.
56. Nakano S, Engel AG. Myasthenia gravis: quantitative immunocytochemical analysis of inflammatory cells and detection of complement membrane attack complex at the end-plate in 30 patients. *Neurology*. 1993;43(6):1167–1172.
57. Lennon VA, et al. Role of complement in the pathogenesis of experimental autoimmune myasthenia gravis. *Journal of Experimental Medicine*. 1978;147(4):973–983.
58. Rouger K, et al. X-Linked Vacuolated Myopathy. *Am J Pathol*. 2001;158(2):355–359.
59. Lo MW, Woodruff TM. Complement: Bridging the innate and adaptive immune systems in sterile inflammation. *Journal of Leukocyte Biology*. 2020;108(1):339–351.
60. Acharyya S, et al. Dystrophin glycoprotein complex dysfunction: a regulatory link between muscular dystrophy and cancer cachexia. *Cancer Cell*. 2005;8(5):421–432.
61. Narasimhan A, et al. Profiling of Adipose and Skeletal Muscle in Human Pancreatic Cancer Cachexia Reveals Distinct Gene Profiles with Convergent Pathways. *Cancers*. 2021;13(8):1975.
62. Deng M, et al. Activation of the Complement System in Patients with Cancer Cachexia. *Cancers (Basel)*. 2021;13(22):5767.
63. Bonetto A, et al. STAT3 activation in skeletal muscle links muscle wasting and the acute phase response in cancer cachexia. *PLoS One*. 2011;6(7):e22538.
64. Barreto R, et al. Cancer and Chemotherapy Contribute to Muscle Loss by Activating Common Signaling Pathways. *Front Physiol*. 2016;7:472.
65. Blackwell TA, et al. Transcriptomic analysis of the development of skeletal muscle atrophy in cancer-cachexia in tumor-bearing mice. *Physiol Genomics*. 2018;50(12):1071–1082.
66. Hillmen P, et al. The complement inhibitor eculizumab in paroxysmal nocturnal hemoglobinuria. *N Engl J Med*. 2006;355(12):1233–1243.
67. Hillmen P, et al. Pegcetacoplan versus Eculizumab in Paroxysmal Nocturnal Hemoglobinuria. *N Engl J Med*. 2021;384(11):1028–1037.

68. Possemato AP, Abell K, Stokes MP. Global Proteome Profiling to Assess Changes in Protein Abundance Using Isobaric Labeling and Liquid Chromatography-Tandem Mass Spectrometry. *Methods Mol Biol.* 2021;2365:301–313.
69. Wessels MR, et al. Studies of group B streptococcal infection in mice deficient in complement component C3 or C4 demonstrate an essential role for complement in both innate and acquired immunity. *Proc Natl Acad Sci USA.* 1995;92(25):11490–11494.
70. Moorwood C, et al. Isometric and eccentric force generation assessment of skeletal muscles isolated from murine models of muscular dystrophies. *J Vis Exp.* 2013;(71):e50036.
71. Abramowitz MK, et al. Skeletal muscle fibrosis is associated with decreased muscle inflammation and weakness in patients with chronic kidney disease. *American Journal of Physiology-Renal Physiology.* 2018;315(6):F1658–F1669.
72. D'Lugos AC, et al. Prior acetaminophen consumption impacts the early adaptive cellular response of human skeletal muscle to resistance exercise. *Journal of Applied Physiology.* 2018;124(4):1012–1024.
73. Huang DW, Sherman BT, Lempicki RA. Systematic and integrative analysis of large gene lists using DAVID bioinformatics resources. *Nat Protoc.* 2009;4(1):44–57.
74. Szklarczyk D, et al. The STRING database in 2017: quality-controlled protein-protein association networks, made broadly accessible. *Nucleic Acids Res.* 2017;45(D1):D362–D368.
75. Krämer A, et al. Causal analysis approaches in Ingenuity Pathway Analysis. *Bioinformatics.* 2014;30(4):523–530.

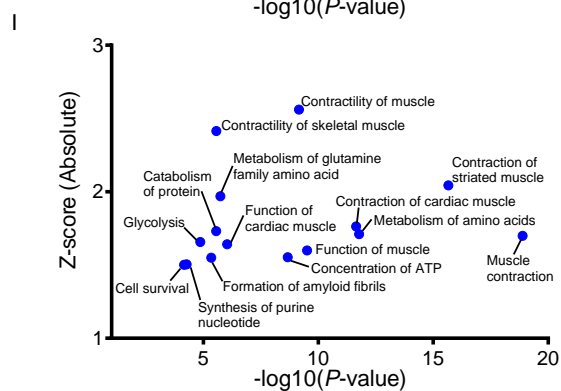
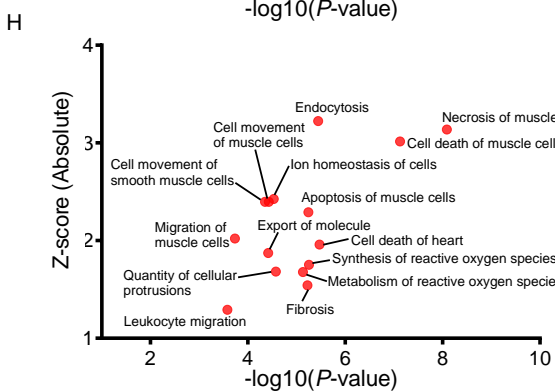
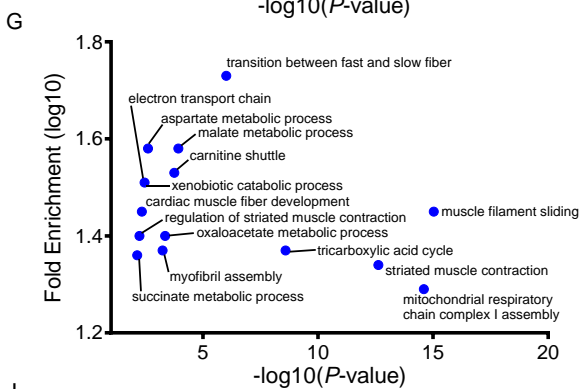
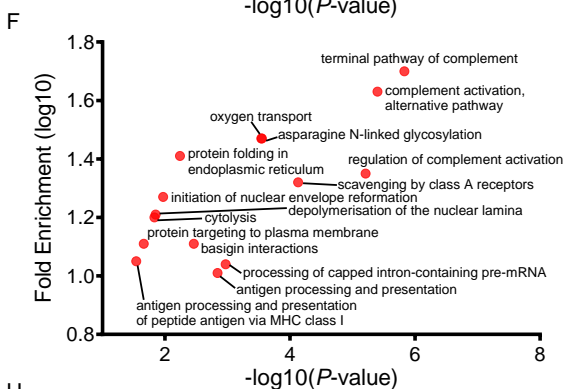
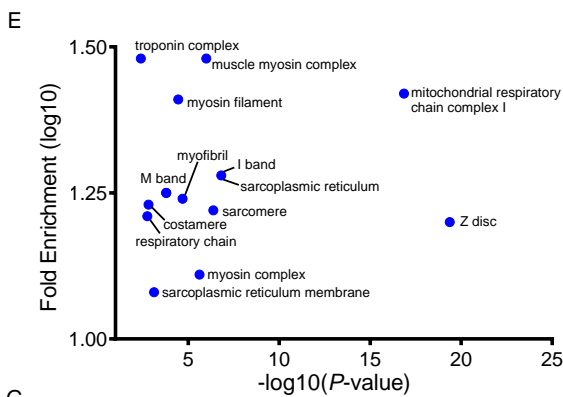
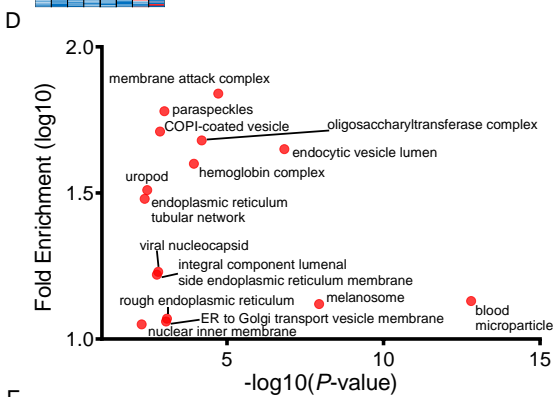
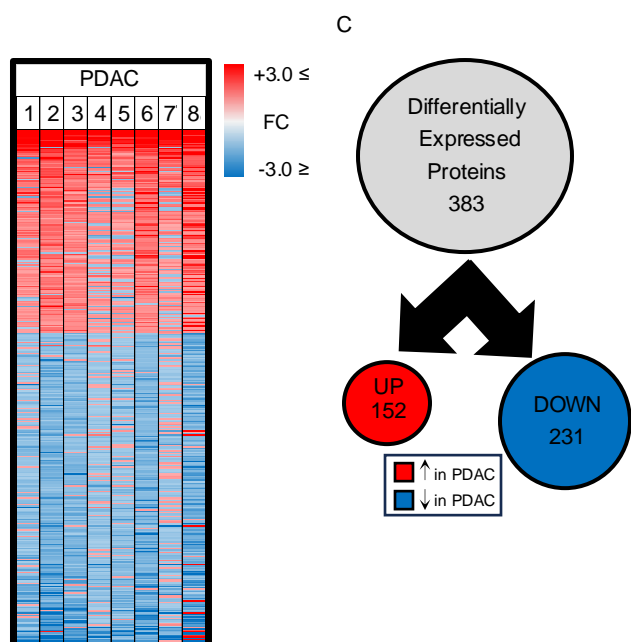
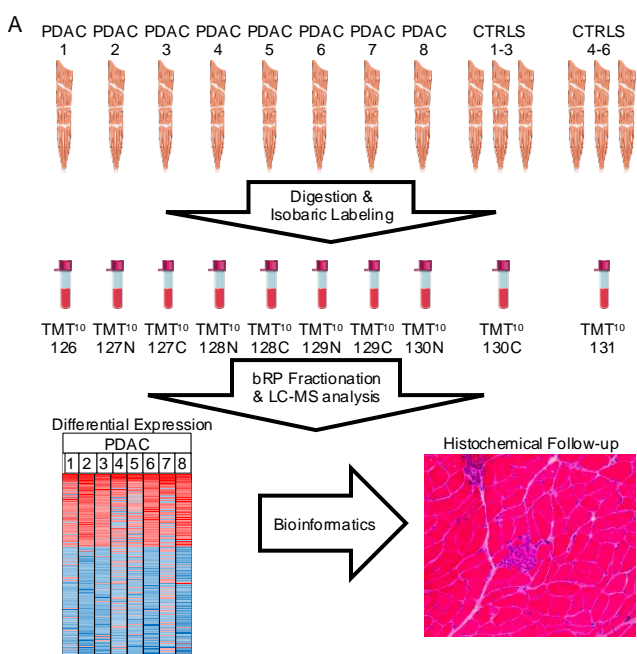


**Figure 1. Skeletal muscle proteome is dysregulated in cachectic pancreatic ductal adenocarcinoma (PDAC) patients.** (A) *Rectus abdominis* biopsies acquired from cachectic PDAC patients (n=8) and non-cancer controls (CTRL, n=6) were subjected to 10-plex Tandem Mass Tag™ proteomics. Biopsies were enzymatically digested to isolate peptides, which were labeled with 10 distinct isobaric tags [8 PDAC + 2 pooled CTRLs (n=6 total)], and combined for LC-MS3 analysis. Differentially expressed proteins between PDAC and CTRL were analyzed through a bioinformatics pipeline, followed by immunohistochemical analyses of skeletal muscle cross-sections. (B) Heatmap displays the relative expression (vs. CTRL) of proteins that met differential expression criteria ( $\geq 2$  peptides;  $-1.25 \geq \text{median fold change} \geq 1.25$ ; FDR-adjusted P-value  $\leq 0.05$ ) between PDAC and CTRL. (C) Among the differentially expressed proteins (DEP; n=383) in PDAC skeletal muscle, most are downregulated relative to CTRL. The top 15 cellular components enriched by upregulated (D) and downregulated (E) proteins were identified through DAVID Functional Annotation. The top 15 biological processes enriched by upregulated (F) and downregulated (G) proteins were identified through DAVID Function Annotations, KEGG and Reactome pathway databases. The top 15 activated (H) and inhibited (I) functions were identified through IPA analysis of up- and downregulated proteins, combined. Annotations with  $< 3$  proteins or a P-value  $> 0.05$  were excluded.

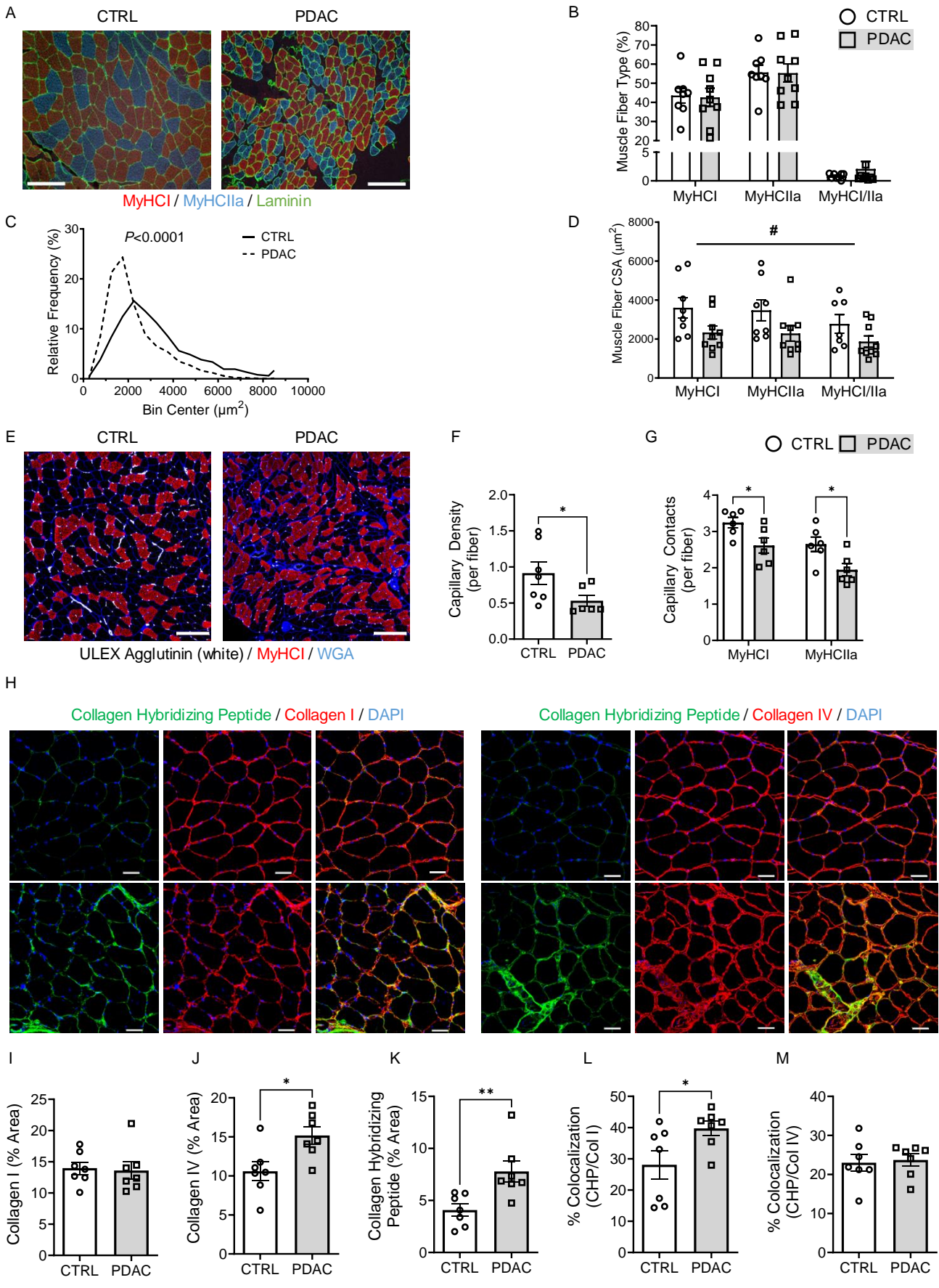


**Figure 2. Skeletal muscle of cachectic PDAC patients exhibits worsened morphology and remodeling of extracellular matrix.** (A) Representative images of *rectus abdominis* cross-sections from CTRL and PDAC stained for myosin heavy chain (MyHC) I (red), MyHC IIa (blue), and laminin (green); scale bar = 200 $\mu$ m. (B) Relative abundance of fibers positive for each MyHC isoform in CTRL and PDAC. (C) Quantification of overall muscle fiber cross-sectional area (CSA) demonstrates a leftward shift in the proportion of small fibers in PDAC vs CTRL. Significance was assessed through a Gaussian least squares regression of binned CSA data and calculating the extra sum-of-squares F test. (D) Fiber type-specific CSA was also quantified. (E) Representative images of skeletal muscle cross-sections stained for endothelial cells (ULEX *europaeus* agglutinating, white), MyHC I (red), and wheat-germ agglutinin (WGA, blue); scale bar = 200 $\mu$ m. Capillary density (F) and fiber type-specific capillary contacts (G) were quantified in CTRL and PDAC (H) Representative images of skeletal muscle cross-sections stained for collagen hybridizing peptide (CHP, green), collagen I or IV (red), and DAPI (blue); scale bar = 50 $\mu$ m. (I-K) Quantification of percent muscle area positive for collagen I (I), collagen IV (J), and CHP (K), as well as quantitative colocalization analyses on cross-sections stained for CHP and collagen I (L) and CHP and collagen IV (M). Data are presented as mean  $\pm$  SEM, with individual data superimposed. Data are representative of n = 7-8 for CTRL and n = 6-9 for PDAC. Differences were assessed using a two-way ANOVA with Sidak post hoc analysis (D,G), Mann-Whitney U test (F) and Student's two-tailed t-test (J,K,L). #  $P < 0.05$  main effect of group, \*  $P < 0.05$ , \*\*  $P < 0.01$ .

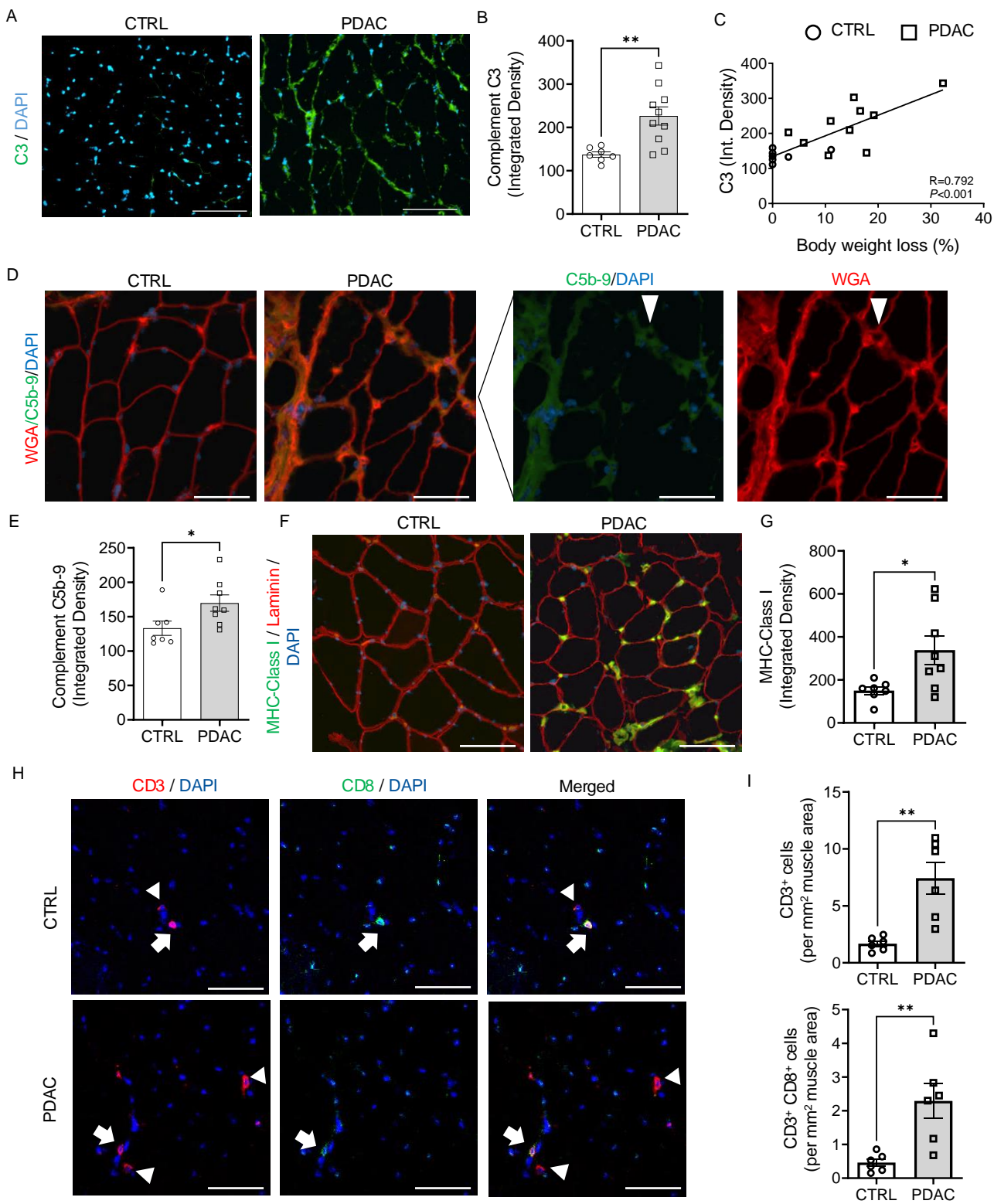


**Figure 3. Complement activation in Skeletal Muscle of Cachectic PDAC Patients.** (A) Representative images and quantification (B) of *rectus abdominis* cross-sections from CTRL and PDAC stained for complement component C3 (green); scale bar = 100 $\mu$ m. (C) Correlation between complement C3 deposition and body weight loss. (D) Representative images and quantification (E) of formation of terminal complement complex C5b-9 (membrane attack complex, green, arrowheads show circumferential staining of endomysial capillaries) in skeletal muscle of CTRL and PDAC; scale bar = 100 $\mu$ m. (F) Representative images and quantification (G) of muscle MHC-I abundance in skeletal muscle of CTRL and PDAC. (H) Representative images of skeletal muscle stained for markers of total T cells (CD3, red, arrowheads) and cytotoxic T cells (CD8, green, arrow); scale bar = 50 $\mu$ m. (I) Quantification of total infiltrating T cells and infiltrating cytotoxic T cells was performed in CTRL and PDAC. Data are presented as mean  $\pm$  SEM, with individual data superimposed. Data are representative of n = 6-7 for CTRL and n = 6-10 for PDAC. Differences were assessed using Student's two-tailed t-test (B,G), linear regression analysis (C), and Mann-Whitney U test (E,I). \*  $P < 0.05$ , \*\*  $P < 0.01$ .

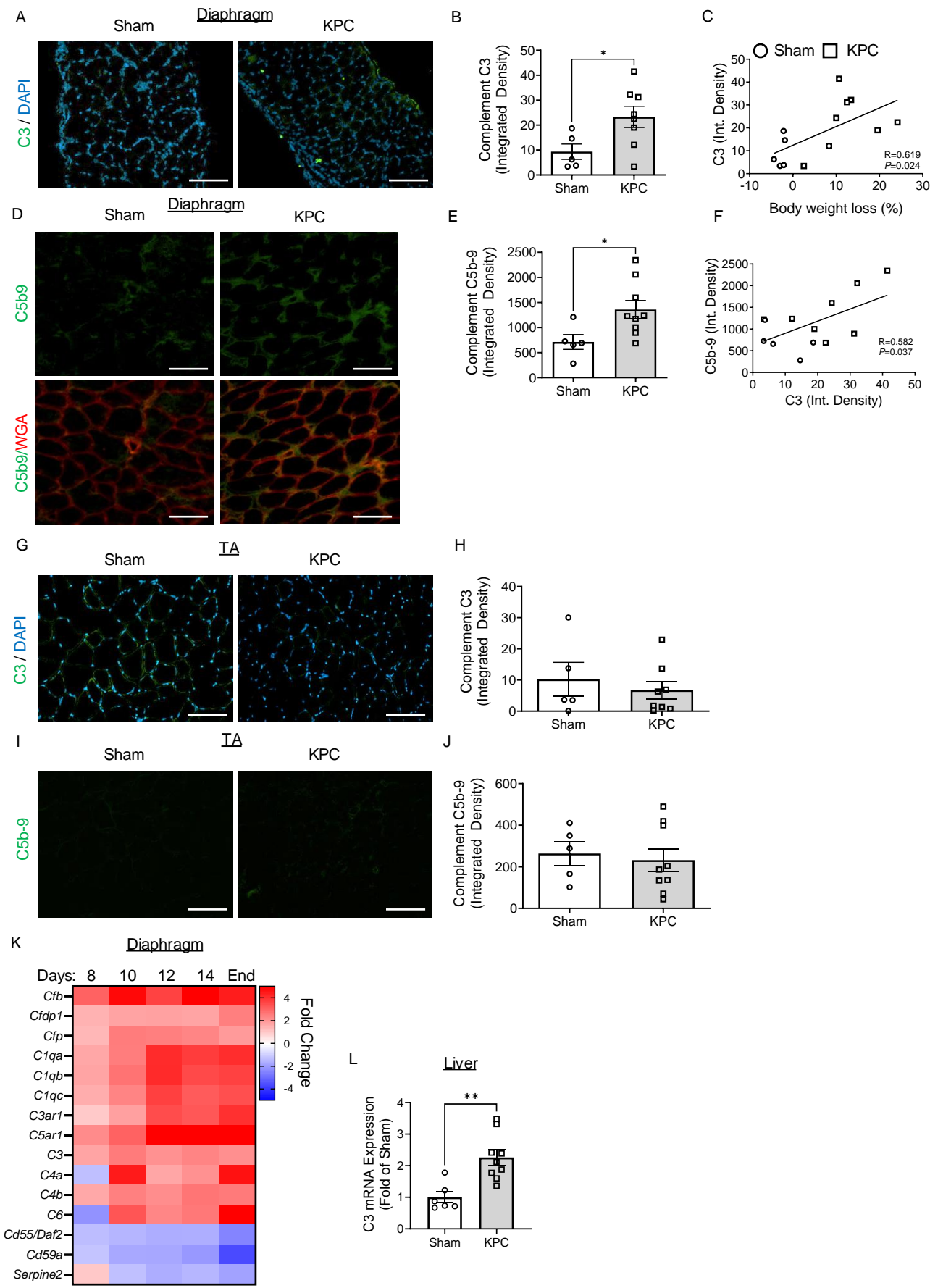


**Figure 4. Orthotopic KPC model of PDAC-associated cachexia recapitulates skeletal muscle complement activation observed in cachectic PDAC patients.** (A) Representative images and quantification (B) of costal diaphragm stained for complement component C3 (green) and DAPI (blue); scale bar = 100 $\mu$ m. (C) Correlation between complement C3 deposition in diaphragm and body weight loss. (D) Representative images and quantification (E) of costal diaphragm stained for terminal complement complex C5b-9 (membrane attack complex, green) and wheat germ agglutinin (red); scale bar = 50 $\mu$ m. (F) Correlation between complement C3 deposition and C5b-9 formation in costal diaphragm. (G) Representative images and quantification (H) of TA stained for complement component C3 (green) and DAPI (blue); scale bar = 100 $\mu$ m. (I) Representative images and quantification (J) of TA stained for terminal complement complex C5b-9 (membrane attack complex, green) scale bar = 100 $\mu$ m. (K) Heatmap depicting changes in the expression level of complement transcripts in the diaphragm muscles of mice with orthotopic KPC tumors during cachexia progression relative to control mice extracted from previously published RNA-seq data by Neyroud et al. (34). (L) RT-qPCR analysis of complement C3 mRNA expression from liver of sham and KPC tumor-bearing mice. Data are presented as mean  $\pm$  SEM, with individual data superimposed. Data are representative of n = 5-9 mice/group. Differences were assessed using Student's two-tailed t-test (B,E,L) and linear regression analysis (C,F). \*  $P < 0.05$ , \*\*  $P < 0.01$ .

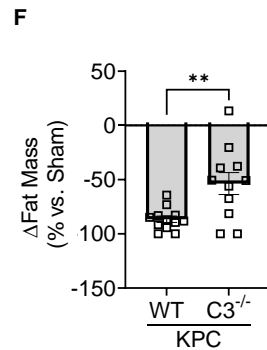
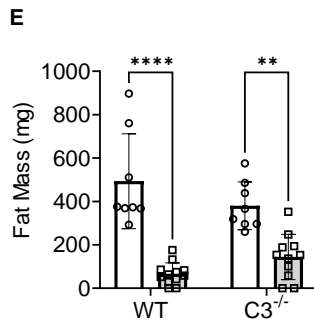
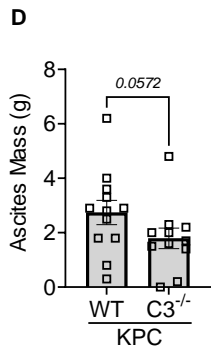
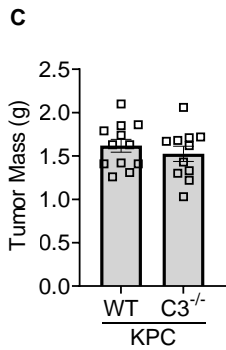
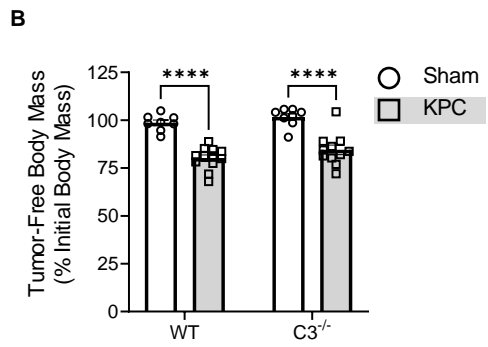
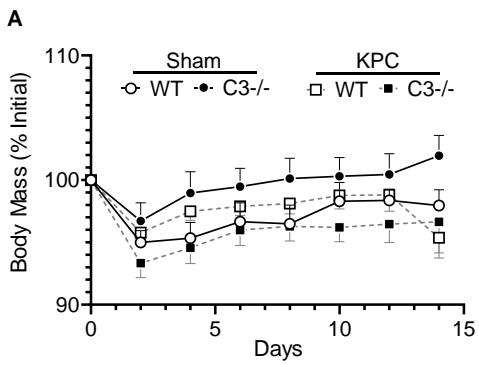


**Figure 5. Deletion of C3 attenuates ascites and fat wasting in murine model of PDAC-associated cachexia.** C57Bl6/J wild-type mice (WT) and complement C3 null C57Bl6/J mice (C3<sup>-/-</sup>) underwent orthotopic surgeries where either PBS (Sham) or KPC tumor cells were implanted into the pancreas. (A) Body mass was monitored over the course of tumor-burden until IACUC-mandated endpoint (day 14). At endpoint, tumor-free body mass (B) was reduced in KPC tumor-bearing mice (squares) versus Sham (circles). Tumor mass (C), ascites mass (D), and fat mass (E-F) on day 14 post-surgery. (F) Tumor-induced fat wasting relative to sham controls was determined within each genotype (WT, C3<sup>-/-</sup>). Data are presented as mean ± SEM, with individual data superimposed. Data are representative of n = 8-12 mice/group. Differences were assessed using a two-way ANOVA with Sidak post hoc analysis (B,E), Mann-Whitney U test (D) and Student's two-tailed t-test (F). \*\*  $P < 0.01$ , \*\*\*\*  $P < 0.0001$ .

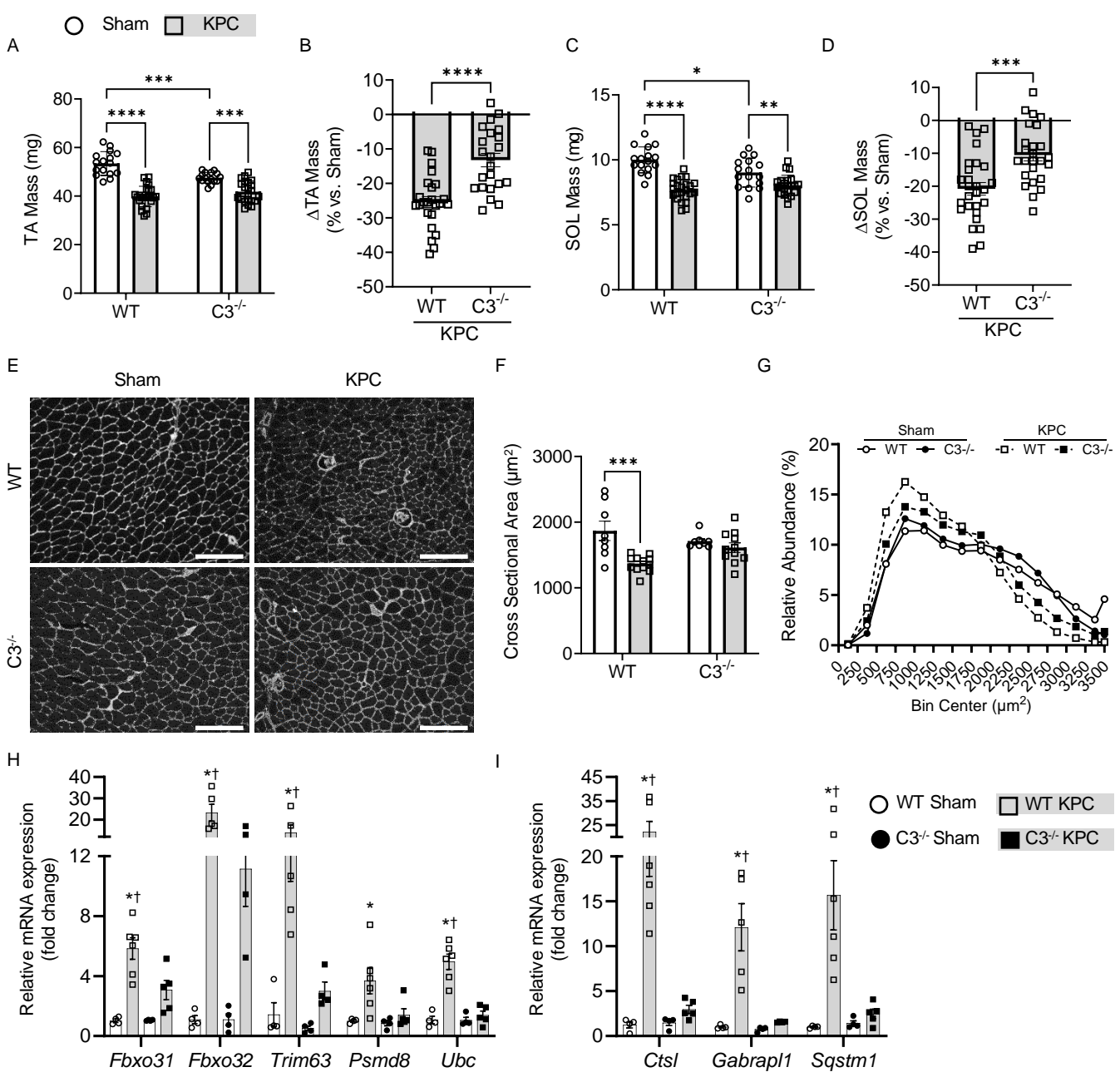


**Figure 6. Deletion of C3 attenuates KPC-induced limb muscle wasting.** (A) *Tibialis anterior* (TA) mass was reduced in KPC tumor-bearing mice (squares) versus Sham (circles). (B) Deletion of complement component C3 attenuated TA muscle wasting. (C) *Solues* (SOL) mass was reduced in KPC tumor-bearing mice, however the deletion of C3 attenuated SOL wasting (D). (E) Representative images of *tibialis anterior* cross-sections stained for wheat-germ agglutinin (white); scale bar = 200 $\mu$ m. (F) Quantification of *tibialis anterior* fiber cross-sectional area (CSA) and (G) distribution of fiber CSA. Data are representative of n = 8-12 mice/group. \*\*  $P < 0.01$ , \*\*\*\*  $P < 0.0001$ . (H) RT-qPCR analysis of atrophy related genes of interest involved in the ubiquitin-proteasome system and the (I) autophagy-lysosomal system in the TA, n = 4-6 mice/group. \*  $P < 0.05$  vs WT Sham group. †  $P < 0.05$  vs.  $C3^{-/-}$  KPC group. Data are presented as mean  $\pm$  SEM, with individual data superimposed. Differences were assessed using a two-way ANOVA with Sidak post hoc analysis (A,C,F,H,I) and Student's two-tailed t-test (B,D).

A

WT

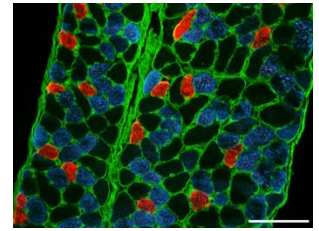
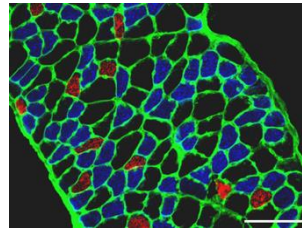
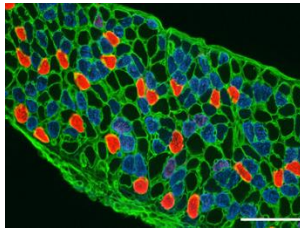
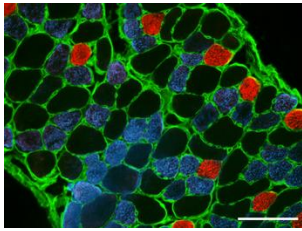
C3<sup>-/-</sup>

Sham

KPC

Sham

KPC



MyHC I / MyHC IIa / Wheat Germ Agglutinin

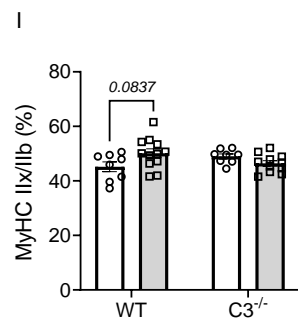
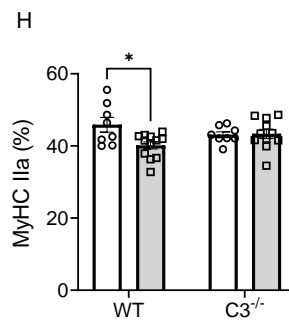
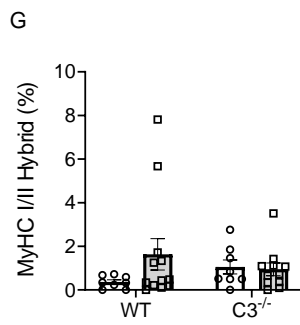
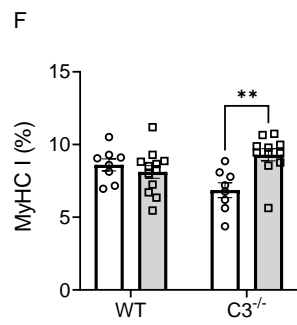
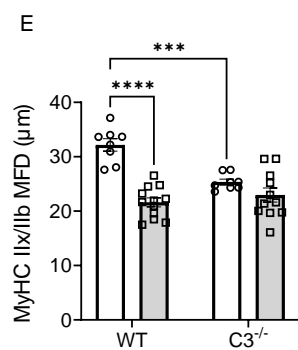
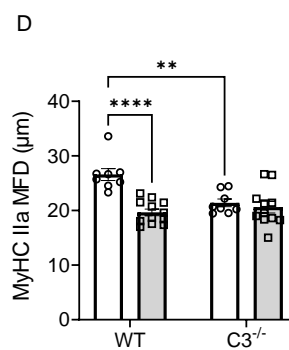
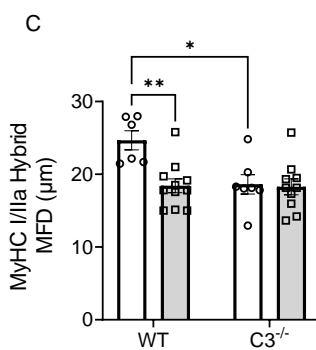
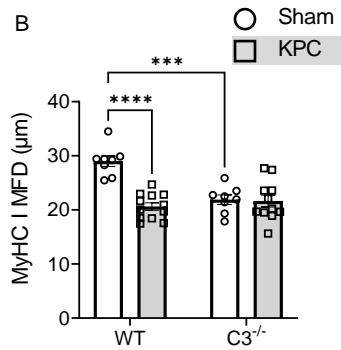


**Figure 7. Deletion of C3 ameliorates KPC-induced diaphragm atrophy and fibrosis.** (A) Representative images of costal diaphragm cross-sections from Sham and KPC tumor-bearing mice stained for myosin heavy chain (MyHC) I (red), MyHC IIa (blue), and wheat-germ agglutinin (WGA, green); scale bar = 100 $\mu$ m. Fiber type-specific muscle fiber size, quantified as minimum Feret's diameter (MFD), was determined for MyHC I fibers (B), MyHC I/IIa hybrid fibers (C), MyHC IIa fibers (D), and MyHC IIx/IIb (unstained) fibers (E). Relative abundance of MyHC I (F), MyHC I/IIa hybrid (G), MyHC IIa (H), and MyHC IIx/IIb fibers (I). Data are presented as mean  $\pm$  SEM, with individual data superimposed. Data are representative of n = 4-12 mice/group. Differences were assessed using a two-way ANOVA with Sidak post hoc analysis. \*  $P < 0.05$ , \*\*  $P < 0.01$ , \*\*\*  $P < 0.001$ , \*\*\*\*  $P < 0.0001$ .

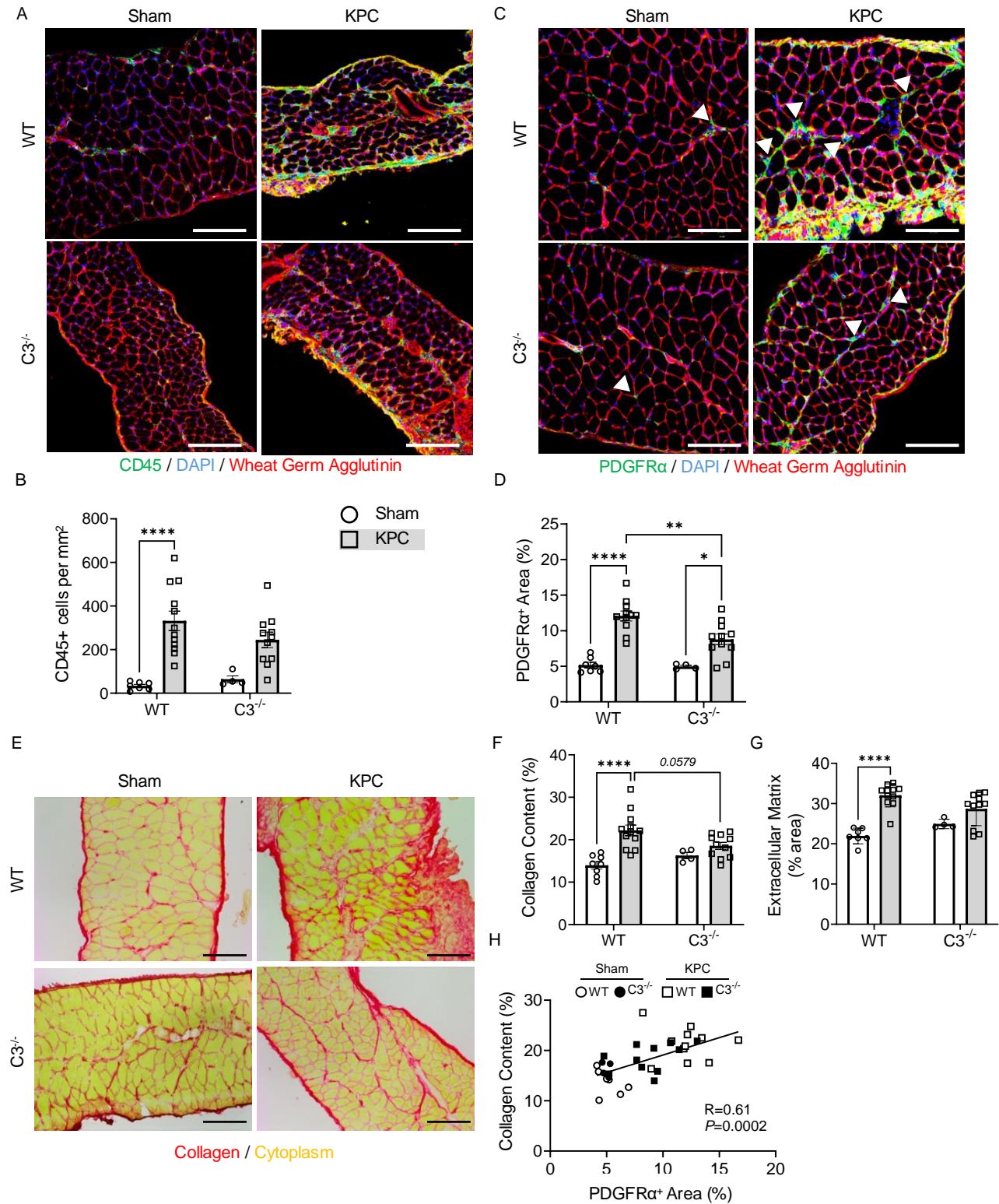


**Figure 8. Deletion of C3 attenuates cell infiltration in diaphragm of KPC tumor-bearing mice.** (A) Representative images of costal diaphragm cross-sections stained for CD45 (green), a pan leukocyte marker, DAPI (blue), and wheat-germ agglutinin (red); scale bar = 100 $\mu$ m. (B) Quantification of the density of infiltrating intramuscular leukocytes. (C) Representative images of costal diaphragm cross-sections stained for platelet-derived growth factor receptor  $\alpha$  (PDGFR $\alpha$ , green) as a marker of fibro-adipogenic progenitor (FAP) cells (white arrow heads), DAPI (blue), and wheat-germ agglutinin (red); scale bar = 100 $\mu$ m. (D) FAP abundance was quantified as muscle area positive for PDGFR $\alpha$ . (E) Representative images of costal diaphragm cross-sections subjected to picrosirius red staining (scale bar = 100 $\mu$ m) for the (F) quantification of total collagen content. (G) Muscle area occupied by extracellular matrix was quantified based on area positively stained for wheat-germ agglutinin. (H) Correlation of collagen content and PDGFR $\alpha$ <sup>+</sup> area. Data are presented as mean  $\pm$  SEM, with individual data superimposed. Data are representative of n = 4-12 mice/group. Differences were assessed using a two-way ANOVA with Sidak post hoc analysis (B,D,F,G) and linear regression analysis (H). \*  $P < 0.05$ , \*\*  $P < 0.01$ , \*\*\*\*  $P < 0.0001$ .

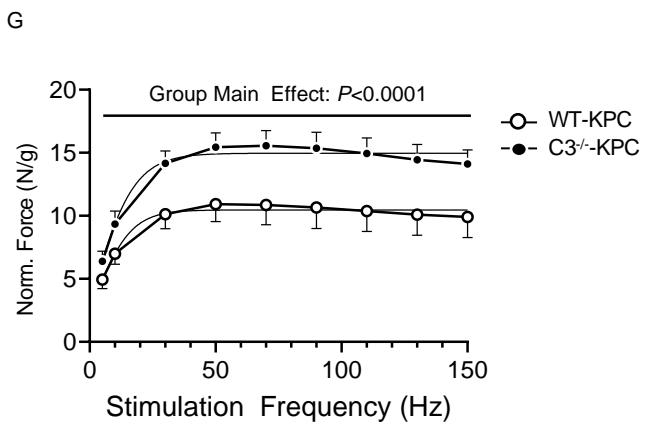
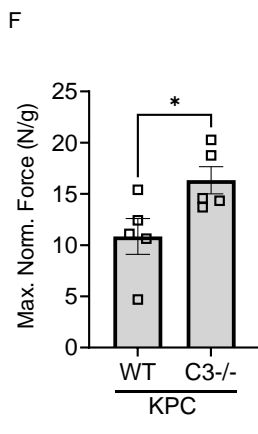
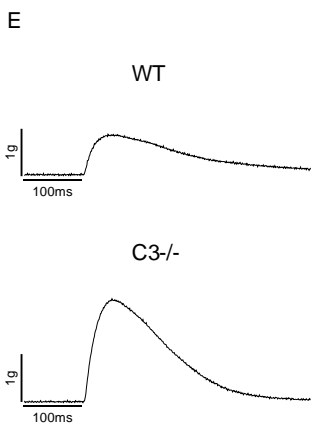
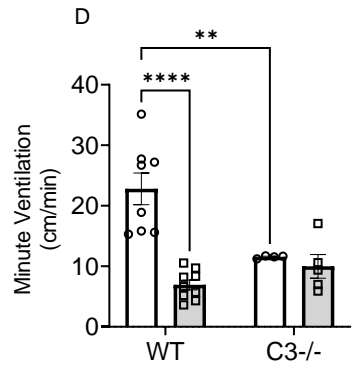
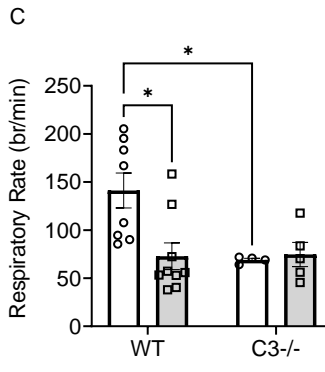
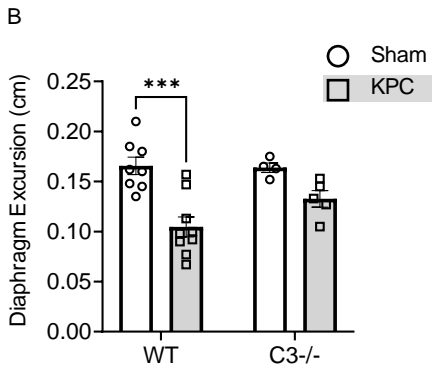
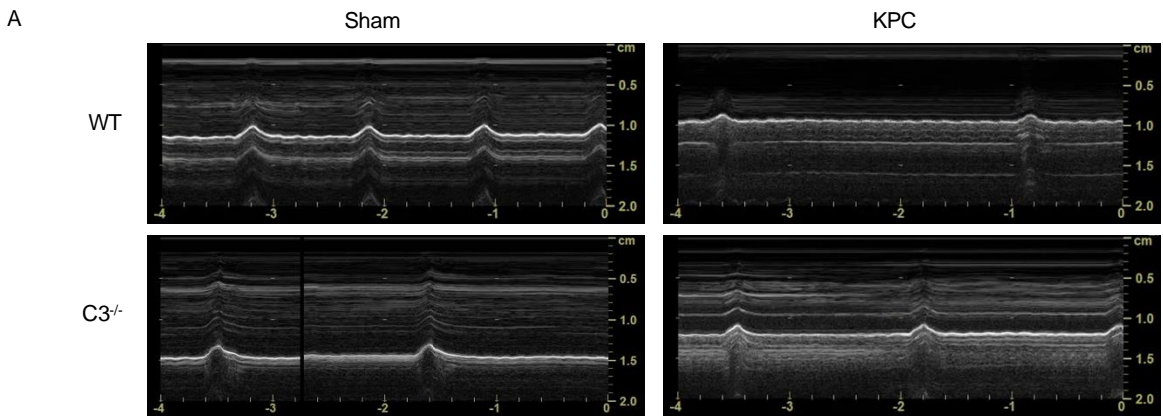


**Figure 9. Deletion of C3 preserves *in-vivo* and *ex-vivo* diaphragm function during KPC tumor-burden.** (A) Representative M-mode ultrasonography traces of *in-vivo* diaphragm contractions at day 14 post-surgery in sham and KPC tumor-bearing mice. M-mode ultrasonography was employed to quantify diaphragm excursion (B), respiratory rate (C), and minute ventilation (D). (E) Representative tetanic force traces recorded from costal diaphragm of WT and C3<sup>-/-</sup> KPC tumor-bearing mice. (F) Maximal normalized tetanic force recorded from costal diaphragm of WT and C3<sup>-/-</sup> KPC tumor-bearing mice. (G) Force-frequency analysis of costal diaphragm demonstrated lower normalized force production in WT mice across a range of stimulation frequencies. Data are presented as mean ± SEM, with individual data superimposed. Data are representative of n = 4-9 mice/group. Differences were assessed using a two-way ANOVA with Sidak post hoc analysis (B,C,D,G) and Student's two-tailed t-test (F). \*  $P < 0.05$ , \*\*  $P < 0.01$ , \*\*\*  $P < 0.001$  \*\*\*\*  $P < 0.0001$ .

Table 1. Human Subject Demographics and Clinical Data

	Age (y)	BMI (kg/m <sup>2</sup> )	6-month BM Loss (%)	SMI (cm <sup>2</sup> /m <sup>2</sup> )	Muscle Attenuation (HU)	Cachexia Grade	Time to Death Post Surgery (m)	AJCC Stage (n)	N Stage (n)	Lymphovascular Invasion (n)
PDAC (n=8)	70 (10)	26.5 (6.2)	15.7 (7.8)	37.2 (7.8)	26.7 (6.8)	II: 1 III: 5 IV: 2	14.8 (13.8)	IIA: 2 IIB: 5 IV: 1	N0: 2 N1: 5	Positive: 6 Negative: 2
<b>Diagnoses (n)</b>										
Non-Cancer Controls (n=6)	66 (9)	31.3 (5.7)	0.0 (0.0)	42.2 (4.9)	29.0 (9.0)					
								Pancreatitis: 1 Bile Duct Stricture: 1 Benign Intraductal Neoplasm: 1 Cholecystitis/Squamoid Cyst: 3		
<i>P</i> -value	0.485	0.166	0.001	0.042	0.607					

Data are presented as mean (*SD*) unless stated otherwise.

## **SUPPLEMENTAL MATERIALS**

**Supplemental Table S1. Expanded human subject demographics and clinical data**

**Supplemental Table S2. Immunohistochemical antibodies, reagents, and oligonucleotides**

**Supplemental File S1. Supplemental Methodology**

**Supplemental File S2. Differentially expressed proteins in skeletal muscle of cachectic PDAC patients**

**Supplemental File S3. RNA-seq data in KPC tumors from WT mice and C3<sup>-/-</sup> mice**

**Supplemental File S4. Supporting Data Values**